Centre for Geo-Information

Thesis Report GIRS-2004-19

Comparison of Scaling-up Methods to Retrieve Chlorophyll Content in Norway Spruce Crowns from Hyperspectral Images Simulated by the DART Model

Christian Martin Ufer Gil

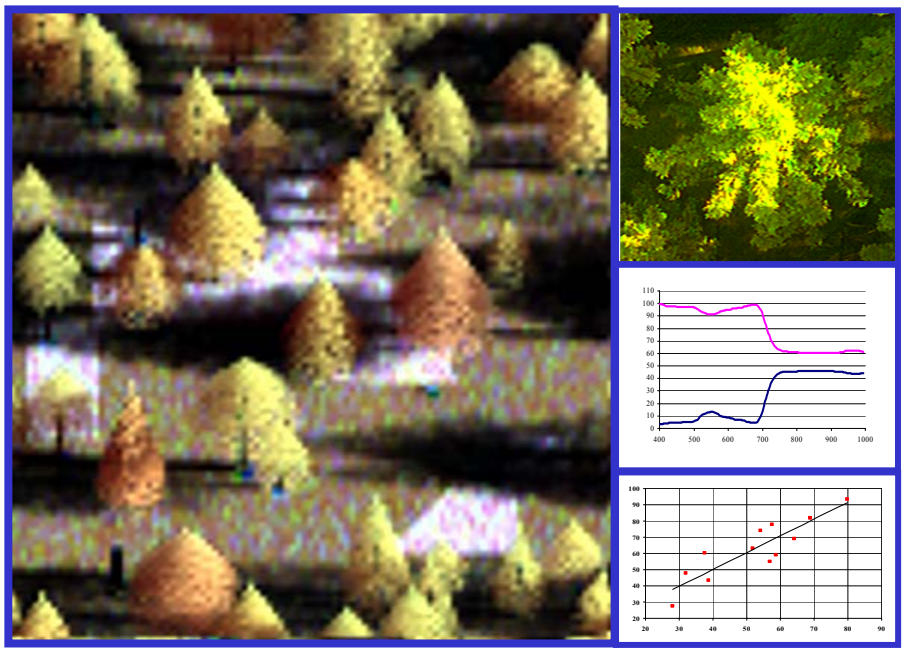

April 2004

WAGENINGEN UNIVERSITY
WAGENINGEN UR

Comparison of Scaling-up Methods to Retrieve Chlorophyll Content in Norway Spruce Crowns from Hyperspectral Images Simulated by the DART Model

Christian Martin Ufer Gil

Registration number 75 02 19 847 130

Supervisors:

MSc. Zbyněk Malenovský
Dr. Jan G.P.W. Clevers

A thesis submitted in partial fulfillment of the degree of Master of Science at Wageningen University and Research Centre, The Netherlands.

February 2004
Wageningen, The Netherlands

Thesis code number: GRS-80326
Wageningen University and Research Centre
Laboratory of Geo-Information Science and Remote Sensing
Thesis Report: GIRS-2004-19

Abstract

The present work was conducted in the core zone of the Sumava Mountains National Park in the Czech Republic. Two field campaigns were performed to obtain the required field measurements of a Norway spruce (Picea abies (L.) Karst.) forest stand. This data was used to simulate hyperspectral images of high spatial resolution (0.90 m.) and to evaluate three different methods to retrieve the chlorophyll content of the Norway spruce crowns. The tested approaches were: (a) scaling-up method using a merit function, (b) scaling-up methods using the neural networks, and (c) scaling-up method of the vegetation optical indices. These methods were evaluated and compared in frame of three different scenarios of varying conditions, being: (1) a "clean" scene without any disturbing factors, (2) a scene with 20% of the additional spectral information of lichens (Pseudovernia sp.) at the crown level and (3) a scene with 20% presence of lichens within the crown and the addition of noise computed in accordance with the signal to noise ratio equal to 5. To simulate these scenarios the discrete anisotropic radiative transfer model (DART) was used to generate the input hyperspectral data for the sensitivity study concerning the chlorophyll content retrievals. The obtained results showed that the overall performance of the scaling-up method using neural networks (cascade propagation generated from BRDF database containing an error of +/- 5%) was the most accurate method. The predicting capabilities of this neural network approach were: scenario 1 (r^2= 0.51 and RMSE = 13.97 μg/cm^2), scenario 2 (r^2= 0.70 and RMSE = 11.69 μg/cm^2) and scenario 3 (r^2= 0.52 and RMSE = 15.99 μg/cm^2). In the case of scenario 1 the best performance was obtained from the scaling-up method using the optical index TCARI/OSAVI (r^2= 0.63 and RMSE = 12.84 μg/cm^2), but when one outlier from the sample values was removed the RMSE of the neural network decreased to 9.54 μg/cm^2 which was the lowest obtained value. It is necessary to note that these results need further testing, because they were carried out using only 13 sample trees, and the comparison of the methods was accomplished only with a nadir hyperspectral image simulated by the DART model.

Acknowledgment

I would like to thank Zbynek Malenovsky for his useful advice and guidance throughout the development of this research project, he also provided me by some of the input data and arranged the use of the DART and PROSPECT models based on an agreement with their authors.

I would also like to thank Jan G.P.W. Clevers from the department of GIS at Wageningen University for his comments and useful advice. Thanks are also going to the researchers from the Laboratory of Forest Ecology, Institute of Landscape Ecology (Academy of Sciences of the Czech Republic) especially Radek Pokorny and Pavel Cudlin for their support in the field data collection and processing.

I will remain deeply indebted to the motivation and encouragement given by my wife during my stay here in Wageningen, and to my family in Guatemala, which supported my studies.

Table of Content

List of Figures

List of Tables

1. Introduction

Norway spruce (Picea abies (L.) Karst.) is one of the most important tree species in Europe. It grows in the north, central and east Europe outside permafrost areas, south to north Greece and west of the Massif Central, France; south of 47° N latitude only in mountains above 400-500 m and ascends to 2200 m in the Balkans. This fast growing species can be identified by a dark green crown with drooping branches and a triangular shape. It is often used for timber production (Frankis, 1999).

In recent years a lot of research has been conducted to determine the causes of spruce forest decline in Europe (Ulrich, 1984). One of the essential bio-indicators of this process is the amount of chlorophyll a and b that is controlled by the tree physiological processes. This bio-indicator should be surveyed at different dates and spatial scales to understand the functioning of forest ecosystems (Demarez and Gastellu-Etchegorry, 2000). Stress of the vegetation decreases the total chlorophyll content causing a change in the proportion of light-absorbing pigments. This allows remote sensing methods, especially in combination with hyperspectral sensors, to identify vegetation stress and classify it by means of the drop of chlorophyll content (Zarco-Tejada, 2001). Hyperspectral sensors are instruments that acquire images in many, narrow and continuous spectral bands. These systems can discriminate among earth surfaces features that have specific diagnostic absorption and reflection characteristics over narrow wavelength intervals such is the case of monitoring the chlorophyll content (Lillesand and Kieffer, 2000).

Extraction of the biochemical information from remote sensing image data has been the purpose of many studies (Haboudane et al., 2002). Most of them rely on empirical or semi-empirical approaches that derive statistical regression equations to estimate the biochemical content of a forest canopy based on their spectral reflectance (Gastellu-Etchegorry et al., 1996; Johnson et al., 1994). An important role, in retrieval of the quantitative parameters from remote sensing image data plays the canopy radiative transfer models. These models are able to relate biochemical and biophysical properties of vegetation to bidirectional reflectance distribution function (BRDF) measurements. This is a key element to the correct interpretation of remote sensing images of terrestrial surfaces (Garcia-Haro and Sommer, 2001).

This study evaluated three different methods to retrieve chlorophyll content in Norway spruce crowns: (1) Scaling-up method a using merit function, (2) scaling-up methods using the neural networks (Combal, 2002), and (3) scaling-up method of the vegetation optical indices (Zarco-Tejada, 2001). To compare the performance of the methods, all of them were evaluated under

different scenarios of varying conditions of interest. The ideal situation would be to gather hyperspectral images where only the biophysical parameter of interest varies while all the other parameters remain constant. This option is difficult to reach in reality, but the canopy reflectance models constitute a unique and powerful alternative (Bruniquel-Pinel and Gastellu-Etchegorry, 1998). Therefore, the DART model simulated the input hyperspectral data for our sensitivity studies about chlorophyll content retrieval.

The discrete anisotropic radiative transfer (DART) model is capable of simulating radiative transfer within 3-D scenes that may include any spatial distribution of trees, soil, water and grass. The Scenes are divided into rectangular elementary cells. Each cell can represent any landscape element (soil, trunk, leaf, grass and others) with specific optical (reflectance, transmittance and phase function) and structural (leaf density) characteristics. All grass and leaf cells are supposed to be made of a homogenously distributed medium. Phase functions of surface (soil, water and trunk cells) and volume (grass and leaf cells) mechanisms can come from field measurements. The space of propagation directions is discretized into contiguous sectors, according to the so-called discrete ordinate theory. Topography, hot spot and multiple interactions (scattering and attenuation) with elementary cells are modeled (Gastellu-Etchegorry et al., 1996).

1.1. Research objective

The main objective is to contribute to the estimation of stress biochemical indicators of Norway spruce crowns by generating knowledge on the best performing methodology to determine their chlorophyll content from remote sensing hyperspectral images.

1.2. Research question

Which is the best performing method to retrieve chlorophyll content in Norway spruce crowns from high spatial resolution hyperspectral data?

1.2.1. Sub-research questions

- What is the accuracy to estimate chlorophyll (Ch_{a+b}) content for Norway spruce crowns by the selected methods?
- Are the methods capable of estimating slight changes in the Ch_{a+b} content ($<15 \mu g/cm^2$)?
- What is the effect of lichen thalluses covering the crowns in the estimation of Ch_{a+b} content by the methods?
- What is the effect of artificially generated noise in the prediction of Ch_{a+b} content by the methods?

1.3. Set-up of the report

Chapter 1 makes a brief description of the research problem and gives the general methodology on what has been done in the present work. The research questions and research objectives are also stated.

In chapter 2 a literature review is conducted in order to have an understanding of the different radiative transfer models currently available for scientific purposes. The chapter presents a detailed description on how the DART and the PROSPECT models work their assumptions and also their performance. An important input for the DART is the estimation of leaf area index (LAI), which is one of the driving forces to obtain an accurate BRDF simulation. The methodology about how to measure leaf area index in the field is explained there. This section also describes the three methods that were applied to retrieve the content of chlorophyll pigments from the canopies of Norway spruce stands.

Chapter 3 describes the methodology used in the present work. The study was conducted at the Sumava National Park (Czech Republic). At this place Norway spruce trees of two categories of chronic multiple stress reaction (resilient-RN and resistant-RT) were selected, and their optical, biochemical, and bio-physical parameters were measured. This information was used as an input for the DART model to simulate a forest stand and consequently three different scenarios of varying conditions of interest were simulated. The chlorophyll content of the trees was estimated by means of three methods, scaling-up of optical indices, merit function and neural networks.

The results and related discussion are presented in chapter 4. The changes made to the physical parameters of the trees to fit the DART model are explained and, the simulated hyperspectral images are represented; a brief study on the performance of DART is also carried out. A comparison at the needle level was performed to determine which of the methods performs better without the effect of the tree structure. The final analyses were made at the level of the canopy to determine the best performing retrieval method.

The conclusions and recommendations are presented in chapter 5. Here the research objective and research questions are answered in order to determine the best performing method to retrieve the content of chlorophyll from a simulated forest stand.

2. Literature overview

2.1. Radiative Transfer Models

The current development of satellite technology and airborne sensors provides improved spatial and spectral resolution of remote sensing data. This data requires careful interpretation that can be done with the aid of reflectance models that describe the complex process of radiative transfer within the vegetation leaf and canopy respectively. A radiative transfer (RT) model should describe the interaction of light with an entity: the reflectance, absorption and scattering. The RT models consist of an abstract and simplified version of reality and they should not rely excessively on unstable mathematical hypothesis (Jacquemoud et al., 2000). A number of canopy bi-directional reflectance models of different complexity have been developed in the past decades. They include simulation models with radiosity and Monte Carlo techniques, geometric models, three-dimensional photon transport models and turbid models among others (Garcia-Haro and Sommer, 2001). Some of them will be discussed in the following sections. It's worth mentioning that the present work only used PROSPECT and DART. The purpose of describing the other methods was to give an overview on how they work and on their performance.

2.1.1. PROSPECT model

The PROSPECT model simulates leaf spectral hemispherical reflectance and transmittance from 400 to 2500 nm as a function of leaf structural parameters and leaf biochemical components such as chlorophyll. Scattering is described by a specific refractive index (n) and a parameter characterizing the leaf mesophyll structure (N). Absorption is modeled using pigment concentration (Ch_{a+b}), water content (C_w) and the corresponding specific spectral absorption coefficients (Ka+b and Kw). With the 3.01 version of the PROSPECT model it is possible to reconstruct, with reasonable accuracy, the leaf hemispherical reflectance and transmittance by adjusting four input variables: *N*, Ch_{a+b}, C_w, and dry matter content (C_m). The advantage of such parameterization may be useful when using models that require leaf optical properties as input parameters to model BRDF at a higher level (Jacquemoud and Baret, 1990).

The simplicity of this model makes it a suitable tool to elucidate the physical and physiological processes controlling the leaf spectral characteristics. However, some of the assumptions limit the accuracy of the model. For example, the model assumes that there is a uniform distribution of water, pigments and structure inside the leaf. Another assumption is that, the angle representing the surface roughness is constant, which is not the case (Jacquemoud and Baret, 1990).

2.1.2. Scattering by Arbitrarily Inclined Leaves (SAIL) model

The SAIL model is a 1D turbid medium radiative transfer model for reflectance prediction of a homogeneous vegetation canopy. The SAIL model assumes that leaf azimuth angle exhibits a random distribution. This assumption is reasonable since only a few plant species have been reported to show definite heliotropic behavior. The only parameters describing the morphology of a canopy layer are the leaf area index, leaf inclination density function and the layer thickness. The model allows to vary the solar zenith angle, LAI and the leaf optical properties of the vegetation in a number of separate wavebands, as well as the reflectance of the soil substrate and the proportion of sky radiance in these bands (Verhoef, 1984).

2.1.3. GeoSail model

The GeoSail model combines a geometric model that calculates the amount of shadowed and illuminated components in a scene with a turbid medium model that calculates the reflectance and transmittance of the canopy. This model combines the SAIL model (Verhoef, 1984) with the Jasinski geometric model (Jasinski, 1990). The SAIL model provides the within-canopy radiative transfer calculations and Jasinski's model combines the SAIL results into a scene reflectance. It is designed to use canopy components such as: optical properties, canopy shape, solar zenith angle and canopy cover. This is done to calculate scene reflectance and the fraction of absorbed or intercepted photo-synthetically activity radiation for e.g. forest stands. GeoSail is based on several assumptions like: all trees have the same shape and size, trees do not shadow each other and the crowns do not overlap each other. The illuminated canopy, illuminated background and the tree shadows each have a single reflectance. The model is limited to nadir views (Huemmrich, 2001).

2.1.4. Parcinopy model

The Parcinopy, is a 3-D radiative transfer model that uses a Monte Carlo ray tracing method to compute the BRDF of vegetation. Photons are thrown from the sun direction. When a photon hits the vegetation or the soil, it can be absorbed, reflected towards another direction for further interactions with the canopy or it can be reflected outside the canopy to contribute to the canopy bi-directional reflectance. About three million rays might be thrown to compute the BRDF's of a given scene. This results in a relative accuracy of 2.5 - 3.0 %. The model requires the canopy architecture to be represented with an ensemble of triangles. Leaves and soil are assumed to be lambertian surfaces (Chelle, 1997).

2.1.5. K-K model

The K-K model is a 3D-leaf canopy transport model that takes into account the architecture of covers. The scene is divided into a rectangular cell matrix and radiation transport is simulated with the discrete ordinate method. The source vector is restricted to propagate in a finite number of directions. The most important drawback of this model is the fact that multiple scattering processes occurring within neighboring cells are neglected. The propagation of cell scattering radiation is always simulated from the center of the cell, causing important errors whenever cells do not have infinitesimal optical depth. Another limitation arises from the hypothesis that discrete directions are equally spaced, which provides far from optimal accuracy (Kimes and Kirchner, 1982.).

2.1.6. Discrete Anisotropic Radiative Transfer (DART) model

The DART is a 3-D radiative transfer model, based on the discrete ordinance method and on an iterative approach. The approach used by DART is comparable with the K-K model. The scene is represented as a rectangular solid medium of adjacent cells forming a matrix. The 3-D radiation regime and the BRDF of 3-D canopies are realistically simulated by considering topography, major physical mechanisms (hot spot), leaf optical properties and four types of scattering. The following section will describe the basic principles of the DART model published by Gastellu-Etchegorry et al. (1996).

A matrix of cells forming a 3-D scene represents a landscape in the DART model. The cells are not required to have equal dimensions and they are identified with the x, y and z coordinates at their center point. Cells are used for simulating different types of scene elements, classified as opaque or solid cells (soil and water) and semi-opaque or turbid cells (trunk, leaf and grass). Each of them requires a specific optical and structural characteristic such as leaf area index, leaf angle distribution, reflectance and transmittance functions. DART cells are simulated as turbid medium with volume interaction mechanisms or solid media with surface and possibly volume interaction mechanisms.

The model processes the interactions of each individual source vector with all encountered cells as it propagates down and up in the scene. During their propagation source vectors meet individual cells. Interaction mechanisms depend on the cell type. Source vectors are transmitted through gaps, totally intercepted by opaque cells or partly intercepted and transmitted by semi-opaque cells. Radiation intercepted by a cell gives rise to scattering and absorption mechanisms. Thus, each cell where scattering mechanisms take place becomes a secondary source.

In a first iteration all direct solar source vectors are processed. They give rise to secondary source vectors in all illuminated cells that are characterized by non-nil scattering phase functions. A solar source vector is processed until it reaches a zero threshold value or encounters a medium where it is totally absorbed and scattered. In a second iteration all source vectors that originate from all secondary sources, and the atmospheric source vectors, are processed. Iterations are systematically conducted for all sources and for all directions. Processing goes on until source vectors escape from the canopy or reach a zero threshold level of flux within the scene.

Once all source vectors have been processed, directional reflectance factors of all upper cells are computed. In a subsequent step the BRDF of each upper cell is resampled in a cylindrical coordinate system for obtaining a cylindrical representation of a hyperspectral image. Depending on the choice of the operator, different types of results can be obtained. For example, if the position, viewing direction and instantaneous field of view of an airborne sensor is known, the DART model can simulate the remote acquisition of spectral images of a specific scene (Gastellu-Etchegorry et al., 1996).

2.1.6.1 Improvements of DART

The DART 1996 version was validated in the framework of the RAMI (Radiation transfer Model Inter-comparison) project (Pinty et al., 2001). The experiment consisted in the comparison of four 3-D reflectance models: Flight (North, 1996), Sprint (Thompsson and Goel, 1998), Raytran (Govaerts and Verstraete, 1998) and DART (Gastellu-Etchegorry et al., 1996). Only BRDFs could be compared because DART is the only 3-D model able to simulate images.

This evaluative work was conducted with a simple landscape: trees on a flat soil. DART was found to be very close to the other models in the visible spectral domain, but difference appeared in the near infrared domain for most view angels. The maximal difference was 11% with a sun zenith angle of $\theta_s = 50^o$. This difference between DART and the other models led to a deep analysis of the approximation DART uses. Three major approximations were stressed out:

1) The location of the middle point (Ms) used to compute scattered radiation is inaccurate
2) The incident radiation that gives rise to multiple scattered radiation is not isotropic
3) The location of points from which scattered radiation propagates is inaccurate.

These 3 major approximations were improved with the aim not to increase computational time. To asses how these changes improved the results, DART simulations were compared to simulations of the reflectance models used in the RAMI experiment. In the near infrared, the spectral domain in which DART differed the most with the other models, the changes decreased

the difference by a factor of three. The maximal difference decreased from 11.1% to 3.2% for $\theta s = 50^{o}$. It was shown that the new changes, introduced into DART, improved significantly its accuracy without increasing the time of computation (Gastellu-Etchegorry et al., 2004).

2.2. Methods to estimate Chlorophyll$_{a+b}$ content in vegetation canopies

Over recent years, expanding research has been conducted to understand the relation between vegetation optical properties and photosynthetic pigment concentration. From the optical point of view, these pigments have a different spectral behavior, with specific absorption features at different wavelengths. The spectral regions that are identified as the most suitable to study chlorophyll are those around 680 *n*m, corresponding to the absorption peak of Ch_a and the region around 550 *n*m that corresponds to the minimum chlorophyll absorption in the visible spectral domain (Haboudane et al., 2002).

The leaf chlorophyll content, low in stressed vegetation, is changing the proportion of light-absorbing pigments. The difference in reflectance between healthy and stressed vegetation due to changes in pigment levels allows the use of remote detections to identify mainly acute vegetation stress by means of mapping it throughout the chlorophyll concentration decline. This relationship is primary through reflectance ratio indices, spectral derivatives and spectral position, particularly in the red edge spectral region. At the leaf level, there has been an emphasis on the identification of optical indices for pigment correlation, bio-indicators and leaf status or vigor. Such relationships have been explored at the canopy level through data from field spectrometers and airborne imaging spectrometers, as well as documenting and exploring the potential confounding effects of canopy structure variables, such as leaf area index (Zarco Tejada et al., 2004). The successful application of leaf-level optical indices by remote sensing requires the progressive development of a link between leaf and canopy optical properties. To establish this relationship, four methodologies have been used:

1) The first method correlated directly the canopy reflectance, measured by remote sensing, with ground-measured pigment concentrations. No leaf reflectance was measured and the link between canopy reflectance and biochemical content was found through statistical relationships. Although significant correlation can be found, no predictive capabilities could be inferred to other study sites since the locally derived relationships are affected by species type and canopy structures (Johnson et al., 1994).
2) The second method used statistically derived leaf-level relationships applied to canopy reflectance for pigment estimation. This method was site and species specific and therefore required a specific calibration for canopy level applicability, which is a function of the

canopy structure and viewing geometry at the time of the remote sensing data acquisition. The reason for this is the difference between the two media: one is where the relationship was derived (leaf) and the other one is where it was applied for the chlorophyll estimations (forest canopy) (Gitelson and Merzlyak, 1997).

3) The third method uses the relationship between the leaf biochemical content and the canopy reflectance. The relation is derived by scaling up optical indices through the canopy reflectance models. An advantage of this method is the use of canopy reflectance models as part of the calculation, avoiding the post-calibration step to compensate for canopy structure or viewing geometry. Therefore, a scaled-up leaf-level statistical relationship can be used directly for bio-indicator predictions on measured canopy reflectance data (Zarco-Tejada, 2001).

4) The fourth method uses the inversion of a canopy reflectance model coupled with a leaf model. In this approach a leaf radiative transfer model uses leaf biochemical components as input to model leaf reflectance and transmittance. This information is used as an input for the canopy reflectance model. The main advantage of this approach is that no leaf sample collection is needed to derive the relationships, but it suffers from the constraint that only the biophysical parameters considered as the leaf-level model inputs can be estimated from measured canopy reflectance (Demarez and Gastellu-Etchegorry, 2000).

2.2.1. Empirical scaling-up method of the vegetation optical indices

The scaling-up methodology is a relationship between leaf biochemical content and canopy reflectance derived by scaling up optical indices through canopy radiative transfer (RT) models. The objective is to derive an algorithm to predict a statistical correlation between sensor reflectance and ground measurements (Zarco-Tejada, 2001) as described in point 3 of section 2.2.

Leaf optical properties (hemispherical transmittance and reflectance) are measured from field data sampling. This information is used to simulate canopy reflectance using a canopy RT model (e.g. DART). Specific derived and/or assumed input parameters resemble the canopy structure, and the angular geometry is defined by the solar zenith, solar azimuth and viewing angles. The canopy spectral bidirectional reflectance factor, simulated through the RT model is used to calculate specific optical indices. For a given optical index a set of optical properties, calculated from the leaf-level spectral measurements, will be used to simulate the canopy BRDF. Leaf bio-indicators measured in each leaf sample (e.g. chlorophyll content) are related to the optical indices calculated from the above canopy-simulated spectra. Therefore, the relationship between

a given bio-indicator and a given optical index is calculated from simulated canopy reflectance rather than from leaf-level measurements.

2.2.2. Scaling-up method using merit functions or neural networks

Radiative transfer models describing the relationship between canopy characteristics and the bi-directional reflectance can be used in the inverse mode to estimate canopy biophysical and biochemical variables. The look-up table method is based on generation of an output table for a discrete set of input parameters covering the expected range of parameters. This approach consists of adjusting the values of input canopy biophysical and biochemical variables **V** such that the BRDF simulated with the radiative transfer model **M** matches the best BRDF measured by the sensor **R**. The model **M** requires a set of *n*var input variables and the corresponding measurement configuration **C** (sun illumination direction, the observation angles and wavelengths) (Combal, 2002). Then

$$\mathbf{R} = M(V,C) + \varepsilon \qquad \textbf{(1)}$$

where ε is the uncertainty counting for both measurement and model uncertainties. It represents the adequacy between the model and the measurements. The simplest way to solve Eq. 1 is to compute and store the graph of the function **M (V, C)**. This look-up table (LUT), containing pre-computed reflectance values, is searched in order to find out the reflectance that most resembles the measured reflectance (Gastellu-Etchegorry et al., 2003). Iterative optimization is the classical technique for inverting radiative transfer models in remote sensing and consists of minimizing a merit function that calculates for instance the root mean square error (RMSE) between the measured and estimated quantities by successive input parameter iteration. Another way how to relate a set of input variables to a set of output variables are the neural networks (NN) composed by two major phases: (a) learning process, and (b) application of the created NN. These nonphysical methods have been shown to be efficient in inversion of canopy models (Combal, 2002).

2.3. Determination of leaf area index in the field

Leaves are the active interface of energy, carbon and water exchanges between forest canopies and the atmosphere. The leaf component of a canopy may be quantified by its structural attributes as leaf area index (LAI). LAI is defined by the one side leaf area per unit of ground area. This important parameter regulates a number of eco-physiological processes, such as for instance evapotranspiration and photosynthesis (Cutini et al., 1997). Direct measurements of canopy structure are tedious and labor intensive; therefore indirect procedures have been

developed. Indirect techniques are based on the close coupling of radiation penetration and structure of the canopy. This theory can be explained as follows:

On a sunny day, the ground beneath a large shaded tree provides an instructive place to contemplate radiative transfer through the canopy. The seemingly uniform shade on the ground is interrupted by sun-flecks. These sun-flecks provide a powerful tool for indirect canopy structure measurements, or better to say the gaps in the canopy that cause the sun-flecks. The gap fraction of a canopy is the fraction of view that is unobstructed by canopy in a particular direction. The sun-fleck fraction is equivalent to the gap fraction at the solar angle. If the foliage in the tree was randomly distributed the probability of interception is proportional to the path length, foliage density and foliage orientation. Then the probability of direct bean radiation passing through the crown without interception T (θ, ϕ) is given by:

$$\mathbf{T\ (\theta, \phi)} = \exp\left(-G\ (\theta, \phi)\ S\ (\theta, \phi)\ \mu\right) \qquad \mathbf{(2)}$$

where θ zenith angle, ϕ azimuth angle, G (θ, ϕ) is the fraction of foliage projected toward direction (θ, ϕ), μ is the foliage density and S (θ, ϕ) is the path length thought the canopy (Welles and Norman, 1991).

A potential problem with indirect radiation techniques is the fact that randomness lies at the hart of simple radiation models, yet foliage position of higher plants, especially trees, is never random. Leaves or needles don't float freely in space, but are arranged along stems or branches in an orderly manner. The branches or stems and the leaves attached to them tend to be separated and distinctive; this apparent clumping effect allows more radiation to pass through unobstructed to the lower parts of the canopy than the random model would predict. In order to correct for this assumptions Chen and Cihlar (1995) defined three major issues in optical measurements of LAI:

1) Leaf angle distribution (LAD): leaf angle distribution is solved with multi-angle measurements with the plant canopy analyzer (PCA) LAI-2000.
2) Leaf spatial distribution: the effect of non-random distribution of foliage is quantified by using a clumping index. Needles in conifer canopies are clumped into shoots (one-year set of needles), branches (assembled from shoots) and tree crowns creating the forest stand canopy. In this case the shoots are threatened as the basic foliage unit, so the clumping is separated into two components:
    a) Clumping of a scale larger than the shoots
    b) Clumping of a scale within shoots

3) Contribution of the supporting woody material to light attenuation: the effect of woody material can be quantified by destructive sampling followed by a relationship between trunk diameter and leaf area to determine wood area (Chen, 1996).

Many optical instruments, such as the PCA, can measure the angular distribution of the canopy gap fraction P (θ), where θ is the zenith angle. From this measurement only the product called effective LAI, denoted by L_e, is obtained as the combination of clumping index (Ω) and the plant area index (L_t). When L_e is measured, L_t can be obtained from:

$$\mathbf{Le} = L_t * \Omega \qquad \mathbf{(3)}$$

where L_t is combined effect of leaf area index (L) and wood area index (L_w) and Ω is a correction factor required to convert L_e to L_t. Note that the smaller the Ω, the more clumped is the canopy. By treating shoots as the basic foliage units, Chen and Cihlar (1995) derived that:

$$\mathbf{\Omega} = \frac{\Omega_E}{\gamma_E} \qquad \mathbf{(4)}$$

where Ω_E is the element clumping index quantifying the effect of foliage clumping at scales larger than the shoot and γ_E is the needle to shoot ratio for the foliage clumping within the shoot. By combining equations (3) and (4) we have:

$$\mathbf{L_e} = L_t * \left(\frac{\Omega_E}{\gamma_E} \right) \qquad \mathbf{(5)}$$

The above equations show that to obtain the true leaf area index (L), three corrections must be applied on the effective leaf area index (L_e), obtained from multi-angle gap fraction measurements (for more detailed information see Chen, 1996).

LAI is an important parameter to model an accurate canopy BRDF. The cell characteristics in DART are defined by LAI, LAD (leaf angle distribution) and foliar optical properties. The DART model uses these input parameters in order to compute the scattering transfer function that characterizes the turbid cells (Gastellu-Etchegorry et al., 1996).

3. Methodology

3.1. Conceptual model

The conceptual model, depicted in figure 1, is showing the general working methodology established for this research project. To be able to simulate the bi-directional reflectance distribution function (BRDF) of a forest stand the optical and structural characteristics of the trees and landscape elements (logs, grasses, bare soil and others) are required as well as their leaf area index and leaf angle distribution. The DART model was used to simulate BRDF of four Norway spruce forest stands, resulting in hyperspectral images. Three different methodologies ((1) scaling-up methods using vegetation optical indices, (2) scaling-up method using merit functions and (3) scaling-up method using neural networks) were applied to assess the Ch_{a+b} content in the frame of three different scenarios. After that an accuracy assessment was performed to compare the predicted values of Ch_{a+b} concentrations with the ground truth. Finally, a statistical analysis was used to evaluate the performance of each method.

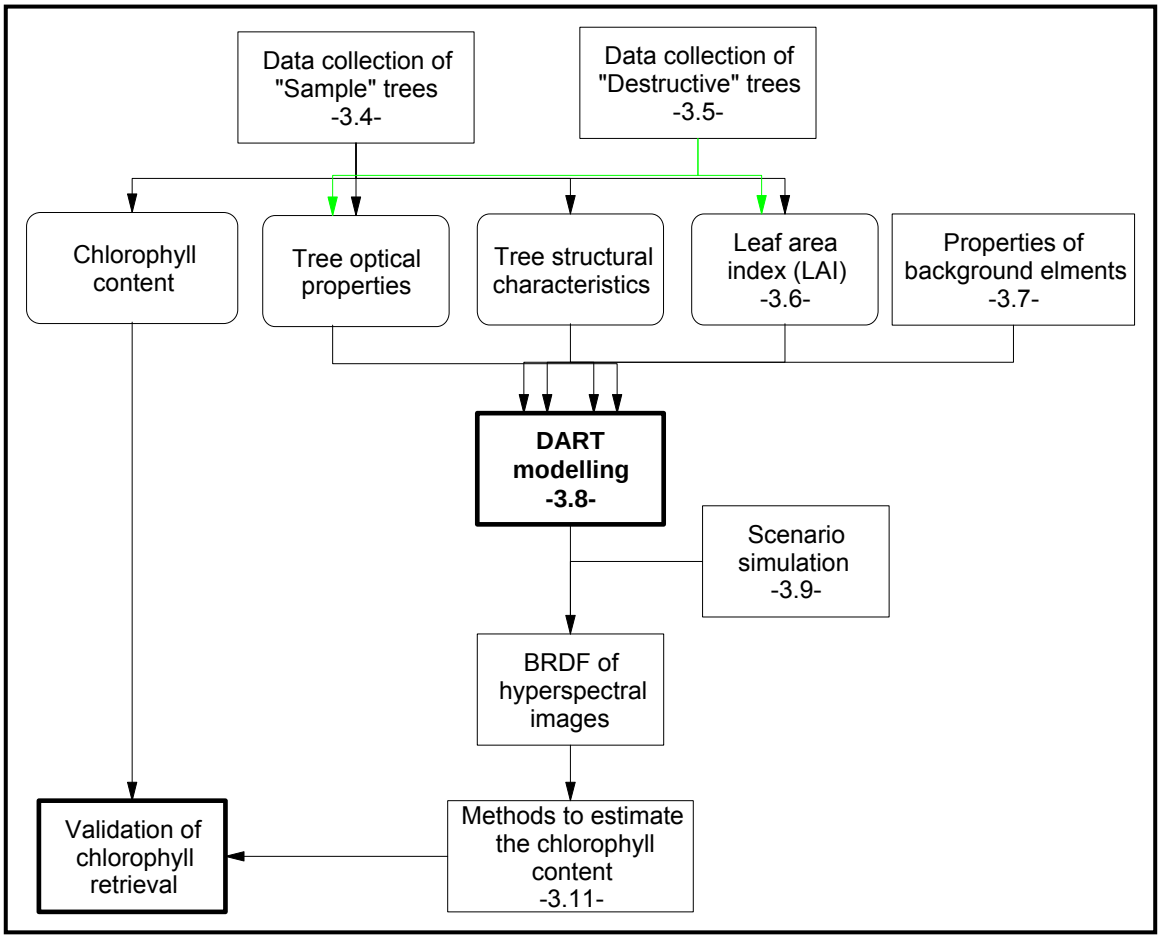

Figure 1. Conceptual model describing the general working methodology.

3.2. Research area

The study area was located near the village of Modrava (48°59'N, 13°28'E), at the Sumava Mountains National Park. This is the largest national park (69,030 Ha.) in the Czech Republic. The National Park is divided into three zones that are supposed to differ in strictness of conservation measures.

1) The core zone (strictly protected) covers 13% of the area and consists of the most valuable natural ecosystems virgin and semi-virgin forest, peat bogs and glacial lakes.
2) The second zone covers 82% of the area and consists of human-affected ecosystems (mostly planted Norwegian spruce). The aim of its management is their re-naturalization and future inclusion into the core zone.
3) The third zone, covering 5% of the park's area, is represented by the human settlements and agricultural land.

The present work was done in the core zone of the national park close to the information center called Breznik. On September 2002 and September 2003 two field campaigns were performed. During that time the field measurements were taken on Norway spruce research plots and later the data was analyzed. Figure 2 shows the location of the research area.

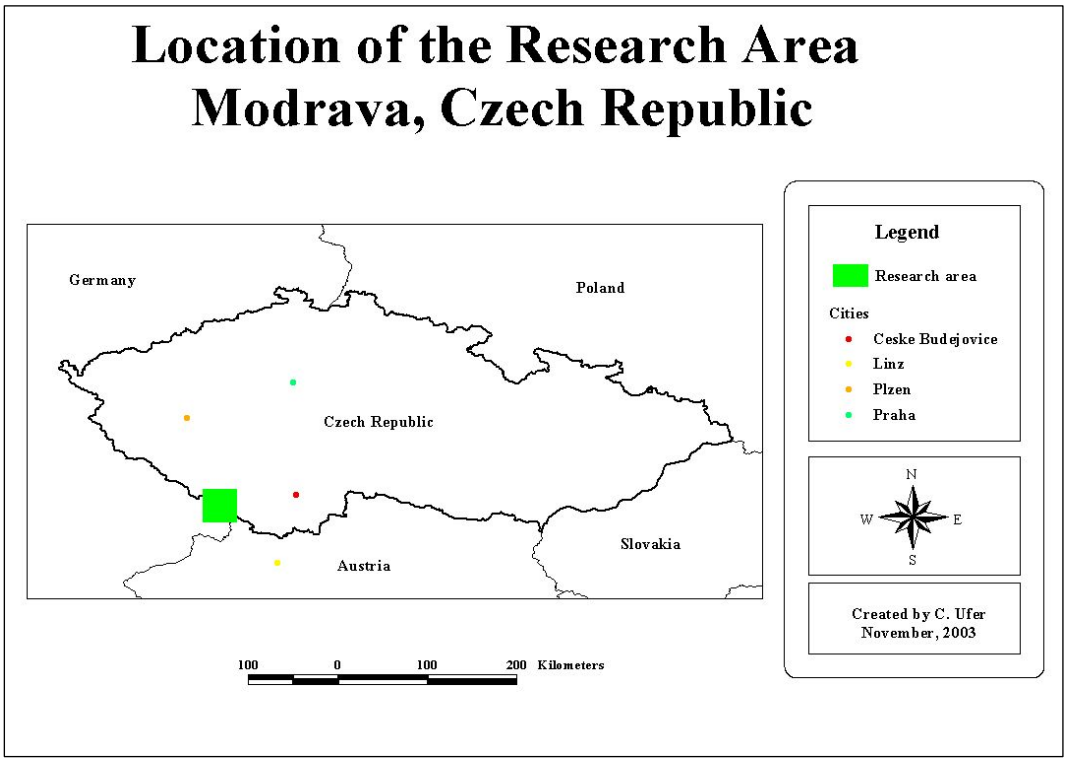

Figure 2. Location of the research area in the Sumava National Park, Czech Republic.

3.3. Selection of Norway spruce trees of interest

Researchers from the Laboratory of Forest Ecology, Institute of Landscape Ecology (Academy of Sciences of the Czech Republic) developed a method to evaluate the response of an individual Norway spruce to multiple stresses. The method is based on the crown transformation and it takes into account the formation of so-called proventitious (secondary) shoots of different orders, which are regenerative shoots initiated by the damage of the foliage. This method also considers the defoliation of the branches. Both characteristics are estimated in the production[1] crown part. Four general categories of multiple stress response can be distinguished based on these bio-indicators, as described in the table 1.

Table 1. Definition of four categories of multiple stress responses of Norway spruce.

Stress response Category	Total defoliation of the production crown part (%)	Secondary Shoots (%)
Resistant tree (non-transformed) RN	≤ 35%	≤ 50%
Resilient tree (transformed) RT	≤ 35%	> 50%
Damage tree non-transformed DN	> 35%	≤ 50%
Damaged tree transformed DT	> 35%	> 50%

In the present work only RN and RT trees were considered. Their selection was made by botanist and ecologist Dr. Pavel Cudlín. In total 17 trees were selected, 8 RN and 9 RT, from them 2 groups were made: (a^2) 13 (6 RN and 7 RT) trees were used to determine the optical properties of needles, the chlorophyll content and their structural biophysical properties (height of tree, crown length, DBH, etc.), and (b^3) 4 (2 RN and 2 RT) trees were used to determine foliage clumping and composition of different age classes of needles.

3.4. Data collection from the sample RN and RT trees

The sample trees were situated inside the forest stands. Four temporal research plots were delimitated around them in accordance with the following criteria:

1) The interest was to simulate the BRDF, so a sufficiently large piece of forest stand was taken to simulate the radiative transfer properly. The trees of interest had to be surrounded by neighboring trees and background elements had to be present. The selection was based on the assumption that each object which could influence the reflectance and transmittance of the

[1] The middle part of the crown, called production crown part, supplies most of the tree assimilate production.
[2] This group of trees will be reference as the "sample" ones
[3] This trees will be reference as the "destructive" ones

tree of interest by means of multiple scattering must be taken into account. Considering this information the plots were established and the locations and allometric properties of all the trees inside the research plots were measured.

2) Each plot must be efficient, this means have as much trees of interest per plot area as possible.

The sample set consisted of 13 Norway spruce trees, 6 RN and 7 RT. Two south[4] branches were cut off per tree by a tree-climber: one branch from the juvenile part and the second branch from the upper level of the production functional part. Three age-classes were sampled for measurements of the optical properties and chlorophyll concentration analysis of the shoots: current year (C), two growing periods old (C+1), and three growing periods old (C+2) shoots. 36 samples were taken from the RN trees: 3 age-classes from 2 branches of 6 RN trees. 63 samples were taken from the RT trees: 3 age-classes from the primary structure (primary shoots) of 2 branches, and 3 age-classes from secondary structure (secondary shoots) of the production branch were sampled within 7 RT trees. Sampled shoots were placed into zip-lock plastic bags, containing moist towel paper, and transferred in a dark cooler to the laboratory for processing.

3.4.1. Measurement of the leaf optical properties

The methodology used to obtain the optical properties was based on Daugtry's method (Daughtry et al., 1989). The LI-COR spectroradiometer Li-1800, connected by optical cable to the integrating sphere 1800-12, was used to collect the hemispherical reflectance and transmittance of the spruce needle samples. The wavelengths used to gather the information were set between 400-1100 *n*m with a step of 5 *n*m, and bandwidth of 1 *n*m. The protocol to measure spruce needles optical properties was modified by Malenovsky et al. (not published). This setup was used as a standard for all the measurements.

The DART model is presently able to work only with one type of foliage optical property per tree crown. Hence we had to make a weighted average of all the optical properties of functional growing parts and age classes to obtain a representative sample. For this purpose we used the information gathered when the destructive sampling was conducted.

3.4.2. Analysis of the chlorophyll content

The needles for chlorophyll content measurement were sampled from the same area where the needles for optical properties were acquired in order to minimize the discrepancy between

[4] The south part is where the tree should conserve better its crown structure, due to more favorable climatic conditions.

these two samples. Because a chlorophyll concentration measurement is a biochemical destructive method, it was not possible to use the same needle set for determination of both: (a) optical properties and (b) chlorophyll content. The sample needles were put in micro-tubes packed into a dark cloth and transported in a cooler at a temperature about of -4^0 C to the laboratory. At their arrival they were frozen at -70^0 C. A sub-sample weighting 0.5 grams was obtained, placed in 10 ml of dimethylformamide and then left in the dark at 8^0 C. for 5 days (Porra et al., 1989). The absorbance from the extract was determined spectrophotometrically at wavelengths of 480, 647 and 664 nm using a Unicam Helios α spectrophotometer. The chlorophyll content was calculated according to the equation of Wellburn (1994).

3.4.3. Optical properties of the woody parts and bark

The optical properties of the woody parts (bark, branches and twigs) were collected during the fieldwork in September 2003. The optical properties were taken by the LI-COR spectroradiometer Li-1800 connected to the integrating sphere 1800-12. Due to the opaque nature of this material only reflectance spectral signatures were measured.

3.4.4. Structural parameters of sample trees

The tree structural data was collected during September 2003. To determine the tree architecture the Laser Rangefinder Impulse 200, combined with the electronic compass MapStar, was used. The data was gathered in a direct electronic way and post-processed by means of the FieldMap software in order to obtain the final information. The acquired and analyzed parameters were:

- Position of the tree: X, Y and Z coordinates were taken. The height (Z) was subtracted or added from the tree height to eliminate the effect of the ground elevation.
- DBH: The diameter at breast height (1.30 m from the tree base) was measured. For trees shorter than 1.3 meters, the diameter was measured where the crown started.
- Height of the tree: the height of a tree was measured from the tree base to the top.
- Bottom of the crown: the lowest starting point of the crown was determined where at least two fully developed branches of the same age whorl were present.
- Circumference of the crown: to calculate the circumference of the crown at least 8 points were taken to determine the perimeter. The ground-points were place in a way that they formed a horizontal drop line from the end of the canopy.

3.5. Destructive data collection from RN and RT trees

During September 2003, four trees (2 RN and 2 RT) were selected and used for destructive observation of several crown structural parameters. Four south branches were taken from each tree: (a) one from the juvenile, (b) one from the upper and one from lower production part, and (c) one from the saturation functional part of the crown. The branches were transported in black plastic bags to the laboratory and analyzed. A destructive approach was conducted to obtain the ratio of growing shoot periods per tree type and the foliage-clumping index per functional crown part. The methodology used to obtain the information by the destructive sampling can be explained as follows:

1) The branches of first order (branch growing directly from the tree trunk) that were 100% defoliated were measured and removed from the sample. Both diameters (at the beginning and ending of this segment of branch) were measured, too.
2) Defining the sample units (SU):
    a) The remaining branch was laid on the floor and then it was divided into segments of 60 cm (branches from production and saturation crown part) or 40 cm (branches of juvenile part). The length was a general rule; the real length depended on the shape and form of each branch.
    b) After that, each segment was divided according to the natural clumps of shoots, into the parts defined as sample units (SU).
3) Each SU was analyzed in a visual way. The presences of four age-classes shoots (C, C+1, C+2 and C+older) per SU were counted.
4) Taken into account this information 10 representative shoots per SU were selected and analyzed in the following way:
    a) 10 shoots were scanned by a desktop scanner to obtain a picture of their projected area. Each shoot was post-processed in order to eliminate the inside gaps between the needles of the shoot and to acquire the real horizontal projected area (not the silhouette of the shoot). The process of shoot scanning had a weak point mainly due to the irregularity of the shape of the needles around the twig. Due to variable distances of the twig to the scanner surface, a low grayscale intensity of some shoots was recorded, which couldn't be detected by the automatic procedure used to calculate the area. This problematic point was solved by manual editing of the scanned shoots.

b) Afterwards the shoots were dipped in liquid nitrogen and the needles were detached from the woody twig.

c) The separated needles were again scanned to obtain their projected area. It is important to mention that each needle had to be facing the surface of the scanner. The remaining needle extension sprigs were removed and all non-needle objects were cleaned from the image during the post-processing of the scanned images. In the final step, the needle-projected area was determined in an automatic way.

d) The projection of the remaining woody twigs was also scanned. The post-processing was done in a way that all the non-twig segments were cleaned from the image; here also the remaining of the needles was removed. As final step, the projected area of woody twigs was automatically measured.

e) Finally, the sample needles and twigs of the 10 representative shoots were oven-dried at 60 °C for 2 days and their dry mass was weighted.

5) The rest of each SU was analyzed in the following manner:

a) The remaining shoots of each SU were placed in dry and dark conditions, so the needles would fall from the twigs.

b) Both needles and woody twigs per SU were dried in a laboratory oven, and their dry matter content was determined.

c) The woody parts of branches with diameter greater than 1 cm were measured separately. Diameters of both ends and the total length were measured to compute the projected area of the wood inside the branch.

6) To upscale the information from shoot/branch level to the tree level, the volume of each functional crown part was determined. The Laser Rangefinder Impulse 200 combined with the electronic compass MapStar was used to obtain the height and radius per functional crown part. The crown profile from the south side of the tree was used for this purpose.

3.6. Measurement of the leaf area index in Norway spruce crowns

3.6.1. Leaf area index of the sample trees

The data to estimate effective leaf area index (L_e) of 13 sample trees was collected during the field campaign in September 2003. L_e was determined by an indirect technique based on the close coupling of the canopy radiation penetration and canopy structure using the Li-Cor Plant Canopy Analyzer (PCA) LAI-2000. The technique combines a measurement of sky brightness from a sensor leveled above the canopy with a second measurement taken beneath the canopy with a

skywards-viewing sensor. The ratio of signal (below/above) is then assumed to be equivalent to the canopy's gap fraction at a specific viewing angle (Welles and Norman, 1991). The PCA sensor was restricted to a horizontal angle of 90° (i.e. one measurement per each geographic direction was required). Four measurements were acquired to obtain the total L_e per tree. This procedure was repeated twice and the average of all measurements was used.

The same procedure as described for L_e was used to estimate the wood area index (L_w), the only difference was that dead trees (100 % defoliated trees) were used. Four trees, freshly defoliated due to the bark beetle attack, were measured and then an average of them was made to obtain mean L_w.

As described in the previous chapter, the measurement from the PCA device is resulting into L_e, so this needs to be corrected in order to obtain L, based on the equation below:

$$\mathbf{L_e} = \left(L * \frac{\Omega_E}{\gamma_E} \right) + \left(L_w * \frac{\Omega_w}{\gamma_w} \right) \quad \textbf{(6)}$$

where L is leaf area index, L*e* is effective leaf area index, Ω_E is element clumping index of a scale larger than the shoots, γ_E is clumping at needle-to-shoot scale. L_w is plant wood area index (100 % defoliated trees), Ω_w is wood element clumping index of the scale larger than shoots, γ_w is supposed to be wood clumping at needle-to-shoot scale. In the computation of the total clumping index for wood area index, the γ_w is dismissed, because first there are no needles in a dead tree and secondly there is just one woody twig present in frame of an age-class shoot (to make a clump at least two woody twigs have to be present). The Ω_w was assumed to be equal to Ω_E (Malenovsky, personal communication). This assumption needs further review to determine the real effect of the wood element-clumping index. Taking into account these assumptions the equation to calculate the leaf area index was finally defined as:

$$\mathbf{L} = \frac{\gamma_E}{\Omega_E}\left(L_e - W * \Omega_E\right) \quad \textbf{(7)}$$

3.6.1.1 Needle-to-shoot area ratio γ_E

Shoots of a conifer forest are distinctive foliage units. Needles, tightly grouped in shoots, are making difficulties to infer the amount of needle surface area from optical measurements. Gower and Norman (1990) used the ratio of projected needles area to the projected shoots area at one

angle as a correction to the PCA measurements to obtain leaf area index. This approach was used and slightly modified according to the following description:

$$\gamma_E = \left(\frac{\text{Projected area of needle} + \text{Projected area of woody twigs}}{\text{Projected area of shoots}} \right) \quad \textbf{(8)}$$

All three variables were generated from samples of the "destructive" trees. The projected area of needles had to be corrected due to the diamond shape of needle cross-section by a specific correction factor in following way: projected area of needles * 2.57/2 (Grace, 1987).

3.6.1.2 Branch element clumping index Ω_E

If shoots would be randomly positioned within the canopy (tree crown) the correction factor needle-to-shoot area ratio should be sufficient to obtain the leaf area index. However, conifer canopies are organized at several levels: shoots, branches, and the crown. Grouping of foliage at these levels results in a canopy gap fraction larger than in the case of a random canopy (Gower and Norman, 1990). The element-clumping index was used to quantify the effect of foliage clumping at the scale of the branch. The following formula was applied to determine one branch element-clumping index:

$$\Omega_E = \left(\frac{\text{Projected area of branch}}{\text{Projected area of shoots}} \right) \quad \textbf{(9)}$$

- Projected area of shoots: this information was generated from the analysis of the branch segments and shoot samples derived from the four "destructive" trees of interest. The total projected area of shoots for the branch (ASB) was computed using the next equation:

$$\mathbf{ASB} = \frac{\left(\sum \text{ASS}\right)\left(\sum D_m \text{SB}\right)}{\sum D_m \text{SS}} \quad \textbf{(10)}$$

  where ASB is area of all shoots in frame of a branch, ASS represents the area of sample shoots, D_mSB is the dry matter of all the shoots from the branch and the D_mSS is the dry matter of sample shoots. 10 representative shoots per sample unit (SU) were analyzed to obtain their projected area as explained earlier in section 3.5. This information had to be up scaled because it was impossible to measure all the shoots from the branch in order to obtain their projected area. Based on this, the shoots for all sample units were oven-dried and their dry biomass was compared to the dry biomass of the whole branch to obtain their projected area.

- Projected area of branch: the projected area of a branch was determined based on the percentage of area occupied by each fully developed branch in the crown horizontal cross-section. A detailed explanation is given in figure 3, where the aerial representations of both the juvenile and the production functional crown parts are depicted.

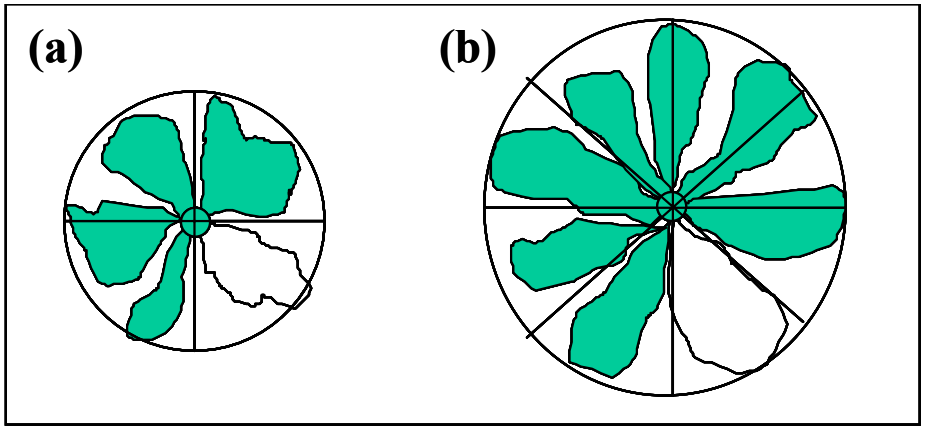

Figure 3. Aerial representations of Norway spruce functional crown parts. **(a) juvenile and (b) production/saturation functional parts.**

The representative sample branch is the white one. Figure 3a shows the horizontal cross-section of a juvenile crown part and 90° sector delineating the area of the branch of interest. The radius of the crown profile at this functional part was used to compute the projected area. Figure 3b represents the horizontal cross-section of a production or saturation functional part of the tree and 45° sectors representing the area of the branch. The radius of the crown profile at this functional part was used to obtain the projected area. It is worth to mention, that this information was obtained based on several very high ground resolution aerial pictures of spruce crowns, taken from a high tower, and the pictures of branches sampled from the four "destructive" trees. Combining all this information the angle representing the area of each branch could be adjusted. However, it appears that this information needs to be more elaborated, because its precision affects significantly the value of the branch element-clumping index. Therefore, the methodological approach to obtain this information should be verified and improved.

3.6.2. Leaf area index (L) of the neighbouring trees

Leaf area index of the neighbouring trees (spruce trees surrounding the sample trees) was estimated through a statistical relationship establish between percentage of total crown defoliation and measured L of the 13 sample trees. The defoliation assessment of all the trees was done

visually by a trained expert ecologist. Total defoliation of the neighboring trees was then placed into the generated regression equation to estimate their individual L.

3.7. Optical and spatial properties of background elements

To model the research plots in a proper way, the optical properties of each ground element that could be detected (elements greater than 0.25 m^2) were measured. For this reason the background surfaces of 4 plots were sampled (one sample per each element was taken). After collecting the samples, they were placed in a zip-lock bag with moist towel paper, inserted in a dark cooler, and transported to the laboratory.

The optical properties were measured in the integrating sphere 1800-12 connected to the LI-COR spectroradiometer Li-1800. A matrix of the observed biological material was placed into the special carrier and measured. In order not to affect the optical properties (mainly transmittance signature) the matrix was created as homogenous as possible, avoiding multiple layers (one layer only) and intermediate holes.

Concerning the spatial composition of the background elements, the botanical composition was drawn by hand in the field per research plot. The tree location and a compass were used to reference each background element and a 2-meter pole lying on the ground as reference was used to maintain the scale. This way a basic schematic land cover map of the area per plot was obtained. Later this information was digitalized and referenced to a local coordinate system. The height of each herbaceous species, its standard deviation, LAD and LAI was estimated by the botanist and ecologist Dr. Pavel Cudlín.

3.8. Modelling hyperspectral images of the Norway spruce research plots by the DART model

The original purpose of the radiative transfer simulation in the DART model was to simulate the spectral information that was generated by an AISA airborne hyperspectral sensor over the Finnish Norway spruce forest during 1999. This AISA imaging spectrometer used was equipped by a CCD matrix of 384 columns and 286 rows. The CCD sensor matrix and the optical system limited the wavelength range from 450-870 *n*m. The row dimension of the CCD array was used for the spectral sampling, resulting in a basic spectral channel width of 1.6 *n*m; up to 5 basic channels can be summed to make channels up to 8.0 *n*m wide (see table 2 containing the band set-up). The spectral resolution along the flight track is determined by the aircraft speed and the exposure time for each raw data row. The nominal aircraft speed when collecting data was 51 m/s and the exposure time was 20.5 milliseconds, resulting in a raw data pixel length of 1.05 meters.

Unfortunately, we did not succeed to get the ground truth information of this image (especially chlorophyll content); therefore we did not use it directly in this study, only the set-up of the bands for the DART simulations remained.

Table 2. Spectral band description of the AISA imagery.

Band No.	Center (nm)	With (nm)	Band No.	Center (nm)	With (nm)
1	452.6	7.3	10	671.3	7.6
2	474.5	7.3	11	700.2	7.6
3	464.9	7.3	12	748.8	7.6
4	524.0	7.3	13	780.7	7.6
5	551.7	7.3	14	800.4	7.6
6	576.5	7.3	15	844.5	7.6
7	601.2	7.3	16	861.2	7.6
8	624.6	7.3	17	870.3	7.6
9	648.5	7.6			

The input parameters required by the DART model to simulate BRDF of the 4 temporal research plots are described as follows:

1) Geometric (directional) parameters:

   The sun position over the research area was calculated for September 15th 2003 at real noon. At that time the sun zenith angle was 42.2o and the sun azimuth angle was 181.2o. These two parameters were transformed to fit the DART setup in the following form:

   a) DART sun zenith angle = 180^o - 42.2^o

   b) DART sun azimuth angle = 360^o - 181.2^o

2) Input parameters of radiative transfer:

   a) Multi-spectral simulations: 12 spectral bands were modeled based on an AISA image. The AISA bands 4-14, with a bandwidth of 8 *n*m, and an additional band placed between bands 11 and 12 (band center at 726 *n*m) were simulated. The DART model itself had a limit in number of spectral bands simulated at once. That was the reason why we had to compute 6 bands in two rounds, which doubled the time demanded to simulate the whole hyperspectral image for one research plots.

   b) Number of interactions of radiative transfer: we specified 4 interactions of radiative transfer to simulate the images. More interactions could yield more reliable result of the simulation, but due to the time constrains the minimum was used. In the last iteration the multiple scattered radiation was extrapolated based on the Gauss-Seidel method.

3) The DART product specifications:

- As outputs the mean bidirectional reflectance function (BDRF) per image was requested. This gave us a matrix based output of the BRDF per band-image with a pixel based energetic status.

4) Input 3-D landscape representations and the surface phase functions:

   - The basic cell size of the representative "maket" (mock-up) of the 3-D research plots was set to be 0.30 X 0.30 X 0.30 meters. The final image (nadir view) was resampled into the cell-size of 0.90 m, so this means we had an average of 9 original cells per one final pixel. The DART algorithm contains a refining routine, which divided the basic cell into 4 smaller regular pixels meaning that the DART cell-size was originally 0.075 m.

5) Soil optical properties:

   - The basic layer of the landscape simulation is soil. The optical properties of soil from the study area (measured in the laboratory) were used. The reflectance was assumed to be lambertian with standard deviation of 0.05.

6) Structural and optical properties of the background elements:

   a) The DART model contains an extension, the vegetation model, which is able to translate automatically a GIS raster layer representing the background elements (herbaceous associations, fallen dead logs, etc.) into a background layer of a DART 3-D representation. A raster map of 0.30 m cell-size made for each research plot (see section 3.7) was used as input for the vegetation model. Unfortunately, the output was too detailed having an unsustainable high number of plots (for example plot number 2 had 1600 polygons at the background). Based on this we decided to generalize the background making the smallest plot of 3.0 X 3.0 meters, maintaining the original cell-size.

   b) Each vegetation type of the background was characterized by a number of biophysical properties (see table 3).

Table 3. Structural description of the vegetation background elements.

Biologic species	Height (m)	STD (m)	LAI	LAD
Calamagrostis villosa	0.5	0.10	1.5	Erectophile
Deschampsia (Avenella) flexuosa	0.17	0.03	1.2	Spherical
Dicranum scoparium	0.07	0.03	1.2	Uniform
Dryopteris austriaca	0.42	0.17	1.2	Planophile
Luzula silvatica	0.22	0.08	1.2	Spherical
Polytrichum commune	0.17	0.12	1.5	Uniform
Sphagnum sp.	0.17	0.12	1.2	Uniform
Vaccinium myrtillus	0.22	0.12	2.5	Planophile

c) To obtain the DART leaf area index (LAI) for each biologic species the following equation was used:

$$\textbf{DART LAI} = \left(\frac{\text{Measured LAI} * \text{Area covered by the specific species per scene}}{\text{Area of whole scene}} \right) \qquad \textbf{(11)}$$

d) Leaf angle distribution (LAD) was determined in accordance with the graphs described in appendix 8.

e) Optical properties of each species were measured in the integrating sphere 1800-12 connected to the LI-COR spectroradiometer Li-1800. The obtained optical properties are described in the appendix 10.

7) Tree crown architectural and optical properties:

a) Percentage of full cells per functional crown part is the main input parameter for the DART model to introduce heterogeneity into the canopy of a tree species. In practice the percentage of full leaf cells in DART is equal to the total clumping index (Ω) of the crown. The total clumping index was calculated by the equation (4) (see section 2.3). Trees of two categories of multiple stress response were analyzed separately and the Ω values for each functional part were obtained. To represent the trees in the DART model as realistic as possible, the tree crown was divided into 10 vertical levels: 1 level for the juvenile part, 3 levels for the productive part and 6 levels for the saturation crown part. The values of foliage clumping per level were introduced in accordance with the measurements (see appendices 2, 3 and 4).

b) DART is able to model different 3-D shapes representing the tree crown. In our case we used the truncated cone for the spruce crown and two sets of four parallelograms to represent the trunk (one outside of the crown and the second one inside of the crown).

Figure 4 shows the difference between a real spruce crown appearance, the measured vertical profile and the DART representation.

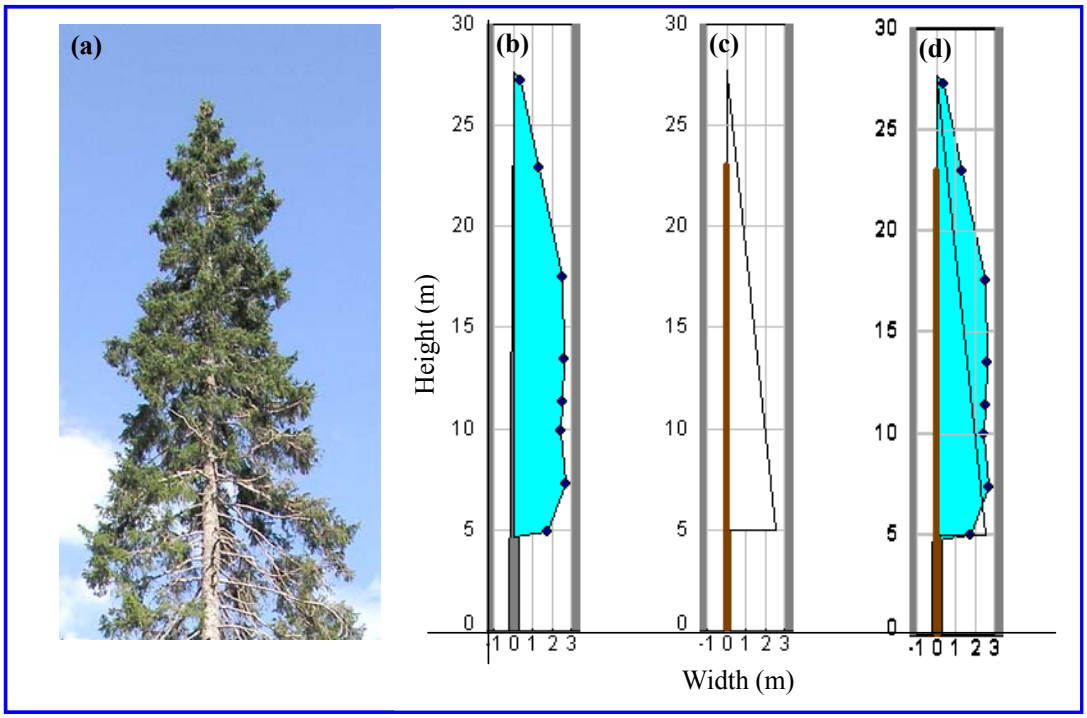

Figure 4. Comparison between the real Norway spruce crown and the crown simulated by the DART model. (a) picture of Norway spruce crown, (b) measured south profile, (c) DART model south profile and (d) comparison between profiles b and c.

The significant difference between the one-side profile of a real spruce tree (blue crown profile, 4b) and the DART generated one (white crown profile, 4c) is clearly visible. To get closer to the real spruce appearance, some changes to the measured data of the trees were introduced. The tree height was reduced by 20%. The crown length was also reduced by 20% for trees with less than 10 meters crown height, and two meters were subtracted from the crowns higher than 10 meters. These changes were taken to reduce the negative effect of the tree crown shape on the radiative transfer simulation. A truncated cone joined with a cylinder should be available in the DART model in order to resemble a more reliable spruce crown shape. The diameter of the trunk was modified in the way that the maximum trunk diameter at the tree top was limited to 0.20 m. The decision about this diameter was based on the cell size, and our intention to avoid seeing the trunk inside of the upper crown part. Figure 4c shows that the upper part of the conic crown had a very narrow diameter meaning that a too thick trunk can strongly influence the RT process simulated at this part. Is worth mentioning that DART is able to handle only one diameter per set of parallelograms (trunk diameter), so an average of the upper

part with the lower part was made for each trunk segment. The trees were classified in four categories as follow:

i) Tree of interest: the LAI was estimated using the PCA device, the Le values were corrected for foliage clumping and then they were directly used as input into the DART model5. The needle optical properties of the crown were computed as the weighted average of the optical properties of the first three age-classes. The weights were equal to the percentage occurrence of each age-class within the spruce crown, obtained during the destructive analysis of four "destructive" sample trees. The distribution of full foliage cells through the canopy was derived separately per stress category RN & RT.

ii) Tree in neighbourhood: LAI was estimated using the regression equation of the tree defoliation compared to the LAI. The trees were sorted into clusters of the DART species based on their LAI (a nominal scale was used to make the clusters). The optical properties were calculated as an average of the "sample" 13 trees of interest. The distribution of full leaf cells within the canopy was also derived as the average of both multiple stress categories.

iii) Young tree: LAI assessment was based on direct expert estimation (the statistical relationship between defoliation and LAI was derived only for adult trees). The optical properties were used as the average of the 13"sample" trees of interest. The distribution of full leaf cells through the canopy was assumed to be equal to the upper part of the crowns of the "sample" trees of interest.

iv) Dead tree: the only possibility to simulate a dead tree in the DART model was to create a trunk with a fractionally small crown (length of 0.50 m and 0.50 m in diameter). To pretend leaf absence a low (neglecting) value of LAI was defined (<0.01). The optical properties were the same as for the neighbouring trees. The distribution of full canopy cells was assumed to be equal to 0.5%. The DART model had some difficulties modeling such unrealistic tree and some cases it was decided to eliminate it from the plot due to an error obtained in the calculation of the hotspot effect.

[5] LAI needs to be transformed into the DART LAI.

3.9. Scenarios of the BRDF simulations

Three different scenarios (see table 4) were performed using the DART simulations. These "virtual" situation, build up on the realistic assumptions were used to determine the best performing method to retrieve Ch_{a+b} content under different conditions.

Table 4. Scenarios of varying condition of interest to be simulated by DART model.

Scenarios	Noise in %	Presence of lichens in %	LAI	Chlorophyll content
1	No	No	Real[6]	Real
2	No	Yes (20)	Real	Real
3	Yes (20)	Yes (20)	Real	Real

1) Scenario 1 represents the real "clean" scene without any disturbing effect. The way how this scenario was obtained is described through the sections 3.2-3.8. This scenario was used as a reference to evaluate the effect of lichens presence in the spruce canopy.
2) Scenario 2 was performed by changing the optical properties of the trees of interest. The optical properties (hemispherical reflectance and transmittance) of most common lichen at the Sumava spruce forests, Pseudovernia sp., were measured by the LI-COR spectroradiometer Li-1800. The final optical properties of the trees of interest resulted from spectral mixing of 80% of the original needle properties and 20% of the lichen optical properties. A visual assessment of 13 "sample" trees of interest was performed in the forest to determine a realistic level of lichens.
3) Scenario 3 was simulated by adding a certain level of noise to the simulated image of scenario 2. The noise simulated in this work tries to resemble only the noise caused by a detector. This kind of noise is due to the discrete nature of radiation. The fact that each hyperspectral system is recording an image by counting photons allows the assumption that this noise can be modeled with an independent, additive model: the noise *n(i,j)* has a zero-mean Gaussian distribution described by its standard deviation and/or variance. This means, that each pixel in the noisy image is the sum of the true pixel value and the random Gaussian distributed noise value (σ_n^2). The intensity of sensor noise in an image is described by the signal to noise ratio (SNR), which is given by

$$\mathbf{SNR} = \sqrt{\frac{\sigma_f^2}{\sigma_n^2} - 1} \qquad \textbf{(12)}$$

[6] Real represents measured values.

where, σ_f^2 is the variance of the real recorded image (in our case the image of scenario 2 plus noise) and σ_n^2 is the variance of the zero-mean noise image (Fisher, 1994). The SNR value was set to be 5 to simulate noise with standard deviation σ_n ~ 20% of the true image standard deviation σ_s . Then σ_n was computed from:

$$\boldsymbol{\sigma_n} = \frac{\sigma_s}{SNR} \quad \textbf{(13)}$$

The IDL function 'gen_image_doit' was used to generate an image with zero-mean noise of σ_n distributed by the Gaussian function per each spectral band. In the final step the appropriate noisy image was summed with the image (scenario 2) of each spectral band at a spatial resolution of 0.90 m.

3.10. Database of BRDF of varying conditions for Norway spruce

A database of BRDF was developed for the purpose to provide an estimation of the chlorophyll content at the level of canopy. Figure 5 shows the general methodology to construct such a database.

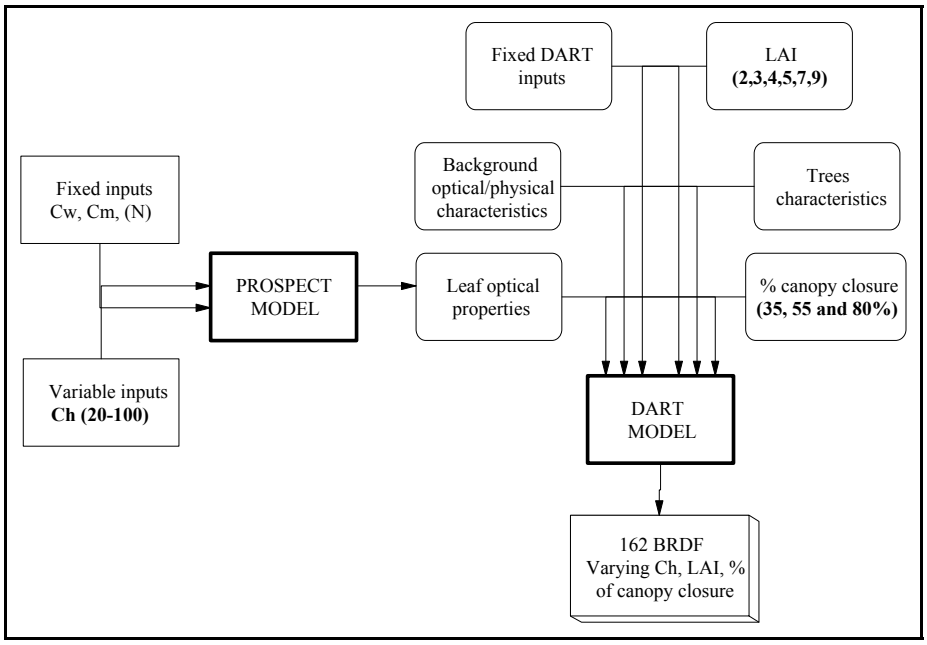

Figure 5. Methodology to generate a BRDF database of varying conditions of interest using the PROSPECT and DART models.

Two RT models were couple for this purpose. First the PROSPECT model was used to generate the Norway spruce needle optical properties for different Ch_{a+b} content and afterwards the DART model was used to upscale this reflectance and transmittance functions to the level of the canopy. The final output was a database of 162 BRDFs varying in Ch_{a+b} content, LAI and percentage of canopy closure (CC).

3.10.1. Simulations in the PROSPECT model

Needle hemispherical reflectance and transmittance were simulated by the PROSPECT model adjusted for Norway spruce by Zbyněk Malenovský in the frame of his PhD study at the Wageningen University. He also provided the fixed input parameters required to simulate the needles optical properties in PROSPECT. His preliminary results are presented in table 5.

Table 5. Biophysical characteristics of Norway spruce needles of two multiple stress reactions.

	Reaction to multiple stress		
	RN	RT	Average
Water content C_w [cm]	0.06	0.06	0.06
Dry matter C_m [g/cm^2]	0.028	0.024	0.026
Leaf structure (N)	2.2	2.1	2.15

Due to time restrictions only fixed average values of C_w, C_m, and N parameters obtained from needles of both RN and RT trees were used for the generation of the database (see table 5). The only free parameter was the Chlorophyll content, varying from 20 μg/cm^2 to 100 μg/cm^2 with a regular increment of 10 μg/cm^2. The outputs were 9 optical properties of Norway spruces needles with a spectral ranging from 400 to 1100 nm at a wavelength interval of 5 *n*m.

3.10.2. Set-up of the DART model to create the BRDF database

Set-up of DART, to model the BRDF database, was the same as described in section 3.8. The only differences were in the canopy structural characteristics and the background, which was entirely represented by the most frequent grass *Calamagrostis villosa*. The allometric characteristics of the trees are described in table 6.

Table 6. Universal tree characteristics for building the BRDF database.

Length of trunk (m)		Trunk diameter (m)		Length of crown (m)	Crown radius (m)	
Outside of crown	Inside of crown	Outside of crown	Inside of crown		Lower part	Upper part
7.75	9.20	0.36	0.19	13.50	2.70	0.00

3.10.3. Canopy closure of the simulated forest stands

Three categories of percentage of canopy closure (CC) were specified to consider different densities of the forest stands. The locations of the universal trees were changed for building up a sub-scene of 35%, 55% and 80% of CC (see figure 6).

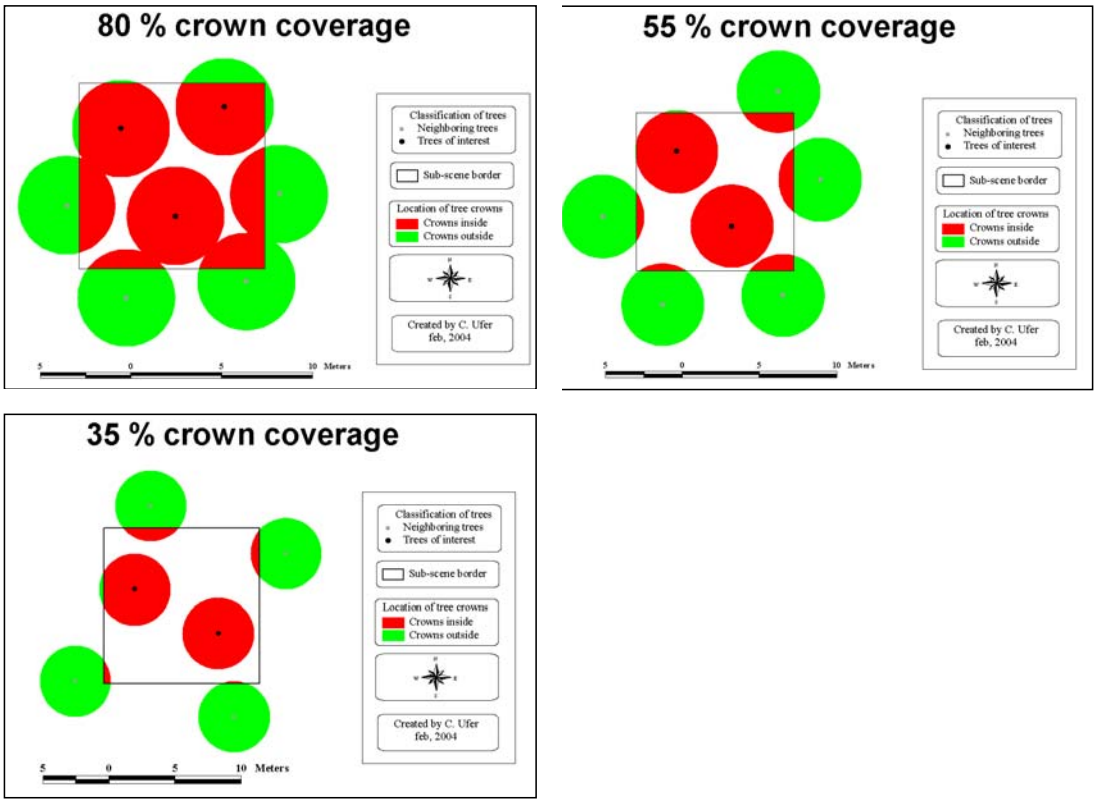

Figure 6. Representation of three different canopy closures for generating the BRDF database.

3.10.4. Simulation of the BRDF database

In a final step 162 DART simulations were carried out to acquire hyperspectral images of the spruce forest stands representing all possible combinations of these inputs: LAI (2, 3, 4, 5, 7 and

9), Ch_{a+b} content (20, 30, 40, 50, 60, 70, 80, 90, 100 µg/cm2) and % of CC (35, 55, 80%). Afterwards degradation of the spatial resolution was performed over all these images to obtain a pixel size of 0.90 m, which resembles the spatial resolution of the AISA image. Finally, the spectral signatures of only sunlit pixels extracted from the crowns of simulated trees, were used to build the reference BRDF database.

3.11. Methods to estimate Chlorophyll content in Norway spruce crowns

3.11.1. Empirical scaling-up method of vegetation optical indices

A reference BRDF database of 162 spruce crown spectral signatures was formed (see section 3.10). Using these information different optical indices was calculated at the canopy level and a predictive scaling-up relationship was established between chlorophyll concentrations and canopy optical indices. The logarithmic scaling-up equation relationship was chosen to estimate chlorophyll concentrations from the different scenarios (Haboudane et al., 2002; Zarco-Tejada, 2001). The vegetation optical indices used for this methodological approach were:

1) Modified chlorophyll absorption reflectance index (MCARI) (Daughtry et al., 2000) defined as:

$$\mathbf{MCARI} = \left[\left(Ref_{700} - Ref_{670}\right) - 0.2\left(Ref_{700} - Ref_{550}\right)\right] * \left(\frac{Ref_{700}}{Ref_{670}}\right) \quad \textbf{(14)}$$

2) Transformed chlorophyll absorption in reflectance index (TCARI) (Haboudane et al., 2002) defined as

$$\mathbf{TCARI} = 3 * \left[\left(Ref_{700} - Ref_{670}\right) - 0.2\left(Ref_{700} - Ref_{550}\right) * \frac{\left(Ref_{700}\right)}{\left(Ref_{670}\right)}\right] \quad \textbf{(15)}$$

3) Ratio between transformed chlorophyll absorption in reflectance (TCARI) index and optimized soil adjusted vegetation index (OSAVI) (Rondeaux et al., 1996) defined as:

$$\mathbf{TCARI/OSAVI} = \frac{3 * \left[\left(Ref_{700} - Ref_{670}\right) - 0.2\left(Ref_{700} - Ref_{550}\right) * \frac{\left(Ref_{700}\right)}{\left(Ref_{670}\right)}\right]}{\left[\frac{\left(1 + 0.16\right) * \left(Ref_{800} - Ref_{670}\right)}{Ref_{800} + Ref_{670} + 0.16\ )}\right]} \quad \textbf{(16)}$$

4) Area normalized to maximal band depth between 700 and 800 nm ($ANMB_{700\text{-}800}$) (Malenovsky, 2003) defined in the following way.

The reflectance signature between 700 and 800 nm is inverted by subtracting the reflectance value from 1. Then the continuum removal procedure described by Kokaly and Clark (1999) is applied on the transformed reflectance, resulting in continuum removed band depths. After that the maximal band depth (MBD) is selected. The area under the continuum-removed inverted reflectance curve (AUC) is calculated based on this equation:

$$\mathbf{AUC} = \frac{1}{2}\sum_{j=1}^{n-1}\left(\lambda_{j+1}-\lambda_{j}\right)\left(\rho_{j+1}+\rho_{j}-2b\right) \quad \textbf{(17)}$$

where ρ_j and ρ_{j+1} are reflectance values at the bands j and j+1 , λ_j and λ_{j+1} are wavelengths of the bands j and j+1; b is the value of the base line, for this case equal to 0; *n* is the number of used spectral bands. The final step to obtain $ANMB_{700\text{-}800}$ is to normalize the AUC by dividing it by MBD.

3.11.2. Scaling-up method using a merit function

In this approach the BRDF database was used to find the measured value that was directly related to a given set of input parameters. The database was sorted according to a cost function; in this case a simple root mean square error (RMSE) was used. To improve the prediction capability of this method a Pearson correlation was first established between wavebands and Ch_{a+b} content. After that only bands having a correlation factor greater than 0.60 were selected for chlorophyll content estimation. It was assumed that bands with lower correlation coefficient would not have a significant prediction capability in the merit function. More likely they could negatively influence the final output by adding additional noisy information not related to Ch_{a+b} content. After selecting the most significant bands the fallowing merit function was applied:

$$\mathbf{RMSE} = \sqrt{\frac{1}{n}\sum_{i=1}^{n}\left(\mathrm{Ref}_{i}-\mathrm{Ref}_{i,db}\right)^{2}} \quad \textbf{(18)}$$

where Ref_i is the BRDF measured for the wavelength *i* from a scenario and $Ref_{i,db}$ is the BRDF obtained from the reference database (PROSPECT + DART). In total nine bands were selected and used in this merit function. After computing all different possibilities, the lowest values (lowest RMSE) was selected (Combal, 2002).

3.11.3. Scaling-up method using Neural Networks

Neural networks (NN) are nonphysical methods that relate a set of input variables to a set of output variables by means of a learning process. The learning task consists of a set of data from which training samples are formed. Each training sample is usually comprised of input data and

desired network response. Applying a neural network to learn this set of data, so called training of the network, requires the user to make a number of decisions related to the use of the available training methods (Logical-designs, 1996).

The learning set was formed from the reference BRDF database (see section 3.10), where an error of +/- 5% was added to the canopy spectral signatures. The testing set was the same database, but without the additional error. The decision to make this set-up was based on the number of samples and the methodology used by Combal et al. (2002) where 2.5 % noise was added to a database of 8000 samples. The decision to increase the error to 5% was based mainly on the low number of samples, because 162 samples is a restricted set of variables. If the noise would not be added then the training and testing datasets would have very high reciprocal correlation, and after running a simulation the difference of errors from testing and training would be 0, which is incompetent. The addition of more information to the set-up of the neural network was also tested, by adding the information about LAI of the trees. Based on this two following learning sets were:

1) Database + 5%e: the selected 9 spectral bands with the addition of 5% error to the reflectance.
2) Database + 5%e + LAI: the selected 9 spectral bands with the addition of 5% error to the reflectance and the information about the leaf area index (LAI).

The setting of the neural network in the ThinksPro software package was time demanding, because there is no general rule to choose the best performing NN architecture. After testing several architectures the best performance was obtained from Cascade correlation learning, with standard input parameters and 10 nodes. The cascade approach is one of the most effective learning methods for supervise learning and for classification problems. It combines the speed of quick propagation with the ability to grow complex multi-layer networks. It is important to mention that the data had to be modified to be able to run this NN architecture. The cascade NN has been designed to perform classification, thus the values of chlorophyll content were needed to be in an interval of 0 to 1; that is why they were divided by a factor of 100. The number of iterations was set to 20000 but the error didn't change already after 15000 iterations.

4. Results and discussion

4.1. Structural characteristics of Norway spruce trees

The "virtual" forest stand was defined in terms of four tree types: (a) trees of interest, (b) neighbourhood trees, (c) young trees and (d) dead trees. The general information displayed in table 7 was obtained from the field campaign in September 2003. This information was corrected and transformed to fit to the DART model inputs. The results of this pre-processing transformation are shown in table 8.

Table 7. Structure characteristics of Norway spruces in the Sumava National Park.

	Crown projection (m^2)		Height of base trunk (m)		Crown length (m)		Tree height (m)		DBH (m)	
Tree type	Mean	Std	Mean	Std	Mean	Std	Mean	Std	Mean	Std
Interest	20.35	7.49	5.02	3.19	22.36	3.29	27.38	2.15	0.53	0.08
Neighbour	12.75	6.97	6.21	3.50	17.51	5.84	23.73	6.86	0.43	0.16
Young	1.59	1.05	0.27	0.15	2.02	1.06	2.30	1.20	0.03	0.02
Dead	1.83	4.24	5.74	3.90	7.79	6.52	13.54	9.18	0.27	0.16

To obtain the original input information (see table 7) the Laser Rangefinder Impulse 200 combined with the MapStar electronic compass was used. The horizontal accuracy of this device was proclaimed by its producer to be approximately 0.2 m. Because the objective of our data collection was to carry out a reliable representation of a Norway spruce forest stand, but not its precise copy, the misplaced tree location (shifted X, Y coordinates) or changes in structural parameters caused by this systematic device error could not affect the results of our work. However, it is worth mentioning that this positioning error was increasing by the equipment reestablishment within the research plots. A central geo-reference point was established after delimitating the plot. Each time when the equipment was moved to another position it had to be re-established and geo-referenced towards this point and so the horizontal error could increase. Therefore it is recommended to maintain the equipment as much as possible at the same position and provide its reestablishment carefully in order to reduce this error.

Table 8. Norway spruces structure characteristics as input for the DART model.

Tree type	Length of trunk in (m)		Diameter of trunk (m)		Length of crown (m)	Radius of crown (m)
	out of crown	inside crown	out of crown	inside crown		
Interest	4.83	11.47	0.51	0.33	20.65	2.48
Neighbour	6.27	6.47	0.40	0.26	15.63	1.95
Young	0.23	0.01	0.02	0.01	1.67	0.68
Dead	4.63	1.54	0.25	0.16	-	-

It was necessary to transform Norway spruce structural characteristics to fit required inputs of the DART model. As mentioned in section 3.8, the height as well as crown length of the tree was reduced by 20% and the height of trees with crown exceeding 10 meters in length was shortened by 2 m. The shape type that was selected to represent Norway spruce crown architecture in the DART model was the truncated cone with an upper radius of 0 cm. When the original data was used to create a 3-D representation of the spruce crowns, the simulated hyperspectral images showed a notable effect of the tree trunk in the upper part of the crown, which did not correspond to reality. Based on this, the modification of the crown structural data was performed. The ratio between radius and crown length was increased from 0.11 cm/m to 0.13 cm/m. Even though this increase, the mentioned effect of the inner trunk was still visible, due to the ratio of turbid foliage cells and non-turbid air cells of very narrow shaped upper crown layers. For example if the ratio of the non-turbid and turbid cells at one of the top crown levels was set to 29% of air cells against 71% of leaf full cells, then the narrow conical crown at the top allowed the trunk to be visible. To correct this disturbing feature the trunk has to be unrealistically shortened. Therefore we would recommend redefining the crown shape templates in the DART.

Rautiainen et al. (2004) studied the effect of crown shape on the reflectance of coniferous stands. In his study the Kuusk-Nilson forest reflectance model was used to evaluate the effect of four crown shapes on a Norway spruce stand. The crown shapes were: (a) ellipsoid, (b) cone, (c) cylinder and (d) cylinder + cone. Comparison of the distribution of single scattering from the tree crowns showed that: the conical crowns had the smallest scattering, cylindrical crowns had the highest, ellipsoid and cylinder + cone were in between. Unfortunately, no comparison was made to the real airborne images of coniferous crowns in order to conclude which crown shape was the best fitting. Based on these findings it would be interesting to make a detailed analysis of the best performing crown shape for Norway spruces using the DART radiative transfer model. In

connection to this a new crown shape template consisting of a cylinder combined with the truncated cone should be added to DART.

4.2. Biochemical and biophysical characteristics of Norway spruce trees of interest

Table 9 describes the biophysical and biochemical characteristics of the 13 "sample" trees of interest from the study area sorted in two categories of multiple stress reaction. The leaf area index was estimated using the PCA device and corrected for foliage clumping by means of the total clumping index. The percentage of defoliation was assessed visually and the chlorophyll concentration was extracted based on the Porra et al., (1989) and the Wellburn (1994) methodologies. The chlorophyll content was a weighted average in terms of the age-classes distribution within the spruce crown and for the three age-classes of needles.

Table 9. Biophysical characteristics of Norway spruces trees of interest.

ID tree	Multiple stress reaction	L_e (PCA)	% of defoliation	Leaf area index (LAI)	Chlorophyll content in $\mu g/cm^2$
5	RN	3.52	60	4.37	60.40
15	RN	3.29	60	3.94	47.96
16	RN	4.55	45	6.32	74.15
17	RN	3.02	65	3.43	77.90
21	RN	4.69	45	6.59	93.55
22	RN	3.77	50	4.85	81.74
6	RT	1.83	60	1.16	58.94
8	RT	3.31	60	3.73	27.56
10	RT	4.51	55	5.82	63.16
11	RT	5.33	45	7.24	43.41
24	RT	6.45	35	9.18	81.79
25	RT	6.27	45	8.87	68.99
29	RT	5.34	50	7.26	55.13

4.3. Hyperspectral images simulated from temporal research plots of Norway spruce forest stands using the DART model

Figure 7 represents the general working methodology to obtain the radiative transfer simulation from the research plots. Figure 7a shows a graphical representation of the input data. Figure 7b shows how this information was transformed to fit the DART model and finally figure 7c represents the output image in RGB false colour composition of the radiative transfer from a 3-D forest stand representation.

(7a)

Representation of Plot # 2 without any changes

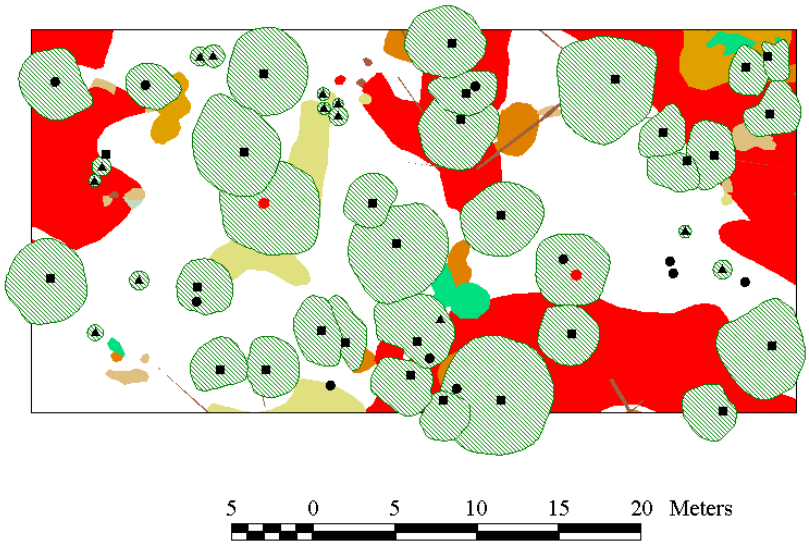

(7b)

Representation of input parameters for DART model of plot # 2

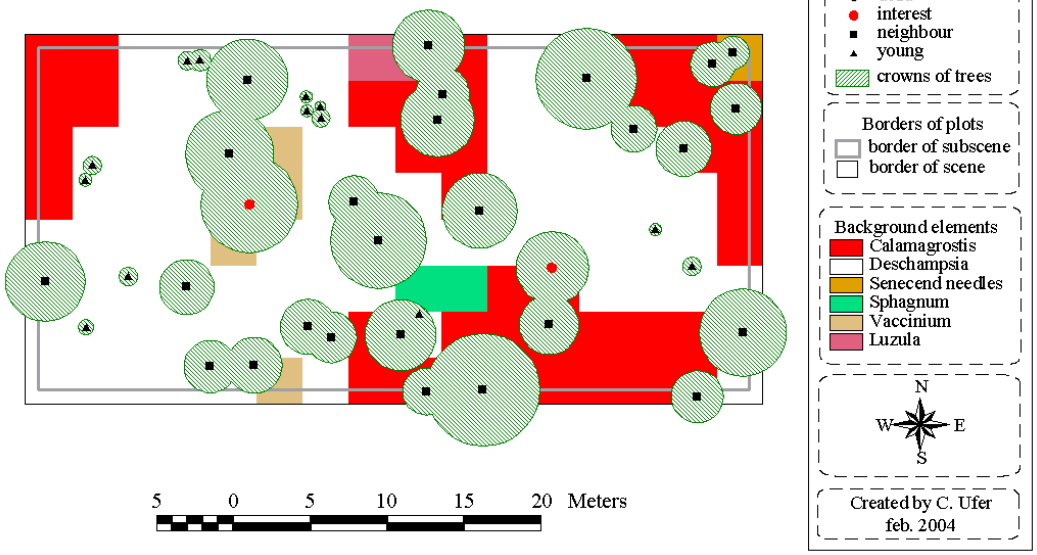

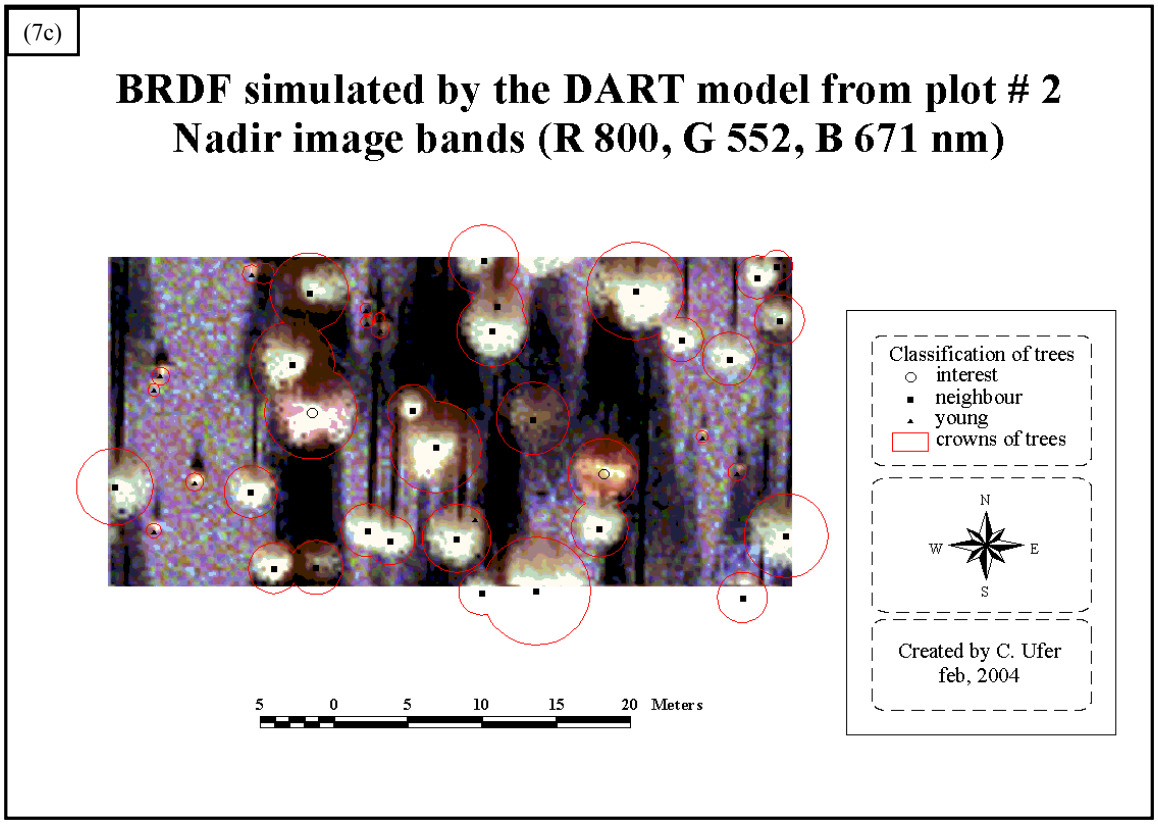

Figure 7. Representation of graphical changes made to the input data to fit the DART model and the radiative transfer simulation from plot #2. (a) input data, (b) transformed data and (C) output data of the radiative transfer simulation.

Figure 7a represents part of a real Norway spruce forest stand. The bottom of the production functional crown part, the widest segment of the crown, was used to determine the crown radius. The shape of the observed crown horizontal projection line was irregular and highly varying. Thus it had to be simplified to a constant radius at the base of the crown. Detailed information was collected in the terrain to express properly the heterogeneity of the forest ecosystem. A map of the background understorey was created to contain every element with an area greater than 0.25 m^2. The DART model was equipped with the software utility called VEGETATION which translated the detailed understorey map into the DART representative pattern containing in case of research plot # 2 around 1600 rectangular polygons of background surfaces. Unfortunately, combination of the RT model with the available computing hardware was not able to handle such detailed information and the simulation crashed due to insufficient computer performance (inadequate processor rate and RAM memory size). The only solution was to generalize the simulations of the scenes. In a first step the objects (understorey) smaller than 5 m^2 in area were removed. Secondly the background elements were resample to the cell size of 3x3 meters. As a result of the generalization the background had a square form and the crowns of the trees had a

constant radius (see figure 7b). Natural variability and heterogeneity was reduced compared to figure 7a to fulfil requirements of the DART RT simulation.

Figure 7c shows the hyperspectral image, as a false colour composition, simulated by the DART (spatial resolution of the image was 0.075[7]m). The original position of the trees and their crown radius are overlaid over the image to clarify the image interpretation. Observing values of the BRDF a dramatic change was found in reflectance near the outside borders of the circles representing the crowns. This might be explained by means of the percentage of turbid leaf cells per functional crown level (see appendix 4) and the spectral mixture with the reflectance of background elements. The percentage of full turbid cells was decreasing from top to bottom of the tree crown, and so the lowest part contained only about 33% of foliage turbid cells. This way the influence of background optical properties (reflectance and transmittance) at these areas increased significantly. Further investigation showed also a shift of the original crown radiuses (tree positions) at the generated images. This minor problem was explained by the rounding performed by the DART. The exact position of the tree was rounded always down to the lower value of the cell size, i.e. the tree at the position of 9.29 m in X coordinate direction was rounded by the DART to 9.00 m and not to 9.30 m. It is important to stress that the resulting scenes of the DART simulation (see figure 7c) represent the "clear" reference image created according to scenario 1. The rest of the simulated images are depicted in the appendix 11.

In general the DART performance was satisfactory. However, the BRDF of the simulated scenes should be compared with the real airborne images to analyse the difference in order to reach clear conclusions about the reliability of the DART simulations. Especially the detail used in this study would make this evaluation interesting, because a forest stand representation of high similarity to the reality was accomplished. While working with the DART model, the following potential improvements that would increase the model performance and operability were recognised:

1) Increase in number of simulated spectral bands: the model is presently limited to simulate 6 bands per simulation. The required number of bands for this work was 12, meaning that each simulation had to be performed twice which increased two times the computational time. Current hyperspectral sensors have the capability to obtain images with several hundreds of spectral bands (e.g. AISA+ sensor in spectral mode acquires 244 bands). To simulate such an

[7] The DART algorithm includes a resampling procedure dividing the original input cell (resolution of 0.30 m) into 4 cells.

image in DART it would require running the model 41 times, which would be inconvenient and time consuming.

2) Sophisticated visualization of the 3-D representation of the landscape: there is a visualization module in DART that allows moving through the 3-D scene and verifying the appearance of its features. In addition to this, it will be useful to have a direct nadir view of the scene to determine and verify the position of the trees and their crown shape. The optical properties of surfaces could be represented by different colours, so the operator would be able to notice where the different background elements are placed and detect differences in optical properties of the trees.

3) New templates of the crown shape: the crown shape that would probably better fit to the architecture of the Norway spruce crown is a cylinder combined with a truncated cone at the top. The cylinder would represent the saturation growing functional part and the truncated cone would represent the juvenile and production part. It would be interesting to compare BRDFs of spruce crowns from a real hyperspectral image with several simulated templates of crown shapes to determine which of them performs most reliably, if no other changes are introduced.

4) Numerous leaf optical properties per crown: the DART model is presently able to use optical properties of only one leaf type per tree crown (species). This fact decreased the reliability of the second scenario where 20% abundance of lichens had to be homogeneously introduced throughout the crown. Such a homogeneous distribution of lichens is far from reality, because they are growing mainly inside the crown (at the defoliated branches) and at the upper part of the crown. If several optical properties of surfaces could be defined in frame of one biologic species, then the DART model would be able to simulate correctly the lichens distribution and furthermore it could simulate properly differences in optical properties of needle age-classes.

5) Variable leaf density within a canopy: leaf density inside the turbid leaf cells is constant within the whole crown, which means the model is not considering properly the spatial variability of the foliage clumping. In appendix 4 measured values of the total clumping index per canopy level are described. As one can see, the upper juvenile part of the crown exposes a very high clumping index of 0.14, meaning that the leaf density there is very high compared to a lower saturation part where the total clumping index is about 0.67. Implicitly the leaf density of the upper crown branches is higher than of branches placed at the bottom of the crown. Foliage clumping is one of the significant structural properties of the canopy,

driving the ratio of the sunlit and shaded needles which is important for photosynthetic processes. For this reason the RT model giving opportunity to specify a vertically and horizontally variable leaf density would be much more universal and closer to reality.

6) Optimisation of the data storage: if the database of the input data was several times edited and saved, the DART started to cumulate useless information. As example, if a simulation was done with the needle optical properties of "non-stressed" RN tree and then the same simulation was repeated with the needle optical properties of "stressed" RT tree, links for both optical properties were stored, even if only the last one was in use. The effect of this redundancy was not investigated, but there is a general trend to optimise any software source code to reach its best potential performance.

4.4. Comparison of the optical indices at the leaf level

An analysis was performed for four selected optical indices (TCARI, TCARI/OSAVI, MCARI and $ANMB_{700\text{-}800}$) at the leaf level, to determine their capability of chlorophyll content prediction. Three input data sets were considered: (a) optical properties simulated by the PROSPECT model, (b) optical properties of the 13 "sample" trees measured during the field campaign in 2002 and (c) optical properties of the same 13 trees mixed in ratio 5:1 with spectral signatures of the most common spruce lichen Pseudovernia sp. The Pearson correlation statistical test was performed to evaluate the reciprocal relation between chlorophyll content of needles and computed optical indices. Results of this statistical test are presented in table 10.

Table 10. Correlation of the chosen optical indices and chlorophyll concentration at the level of needles.

	PROSPECT data		Scenario 1 (real data)		Scenario 2 (plus lichens)	
Optical Indices	R*	Sig.**	R	Sig.	R	Sig.
TCARI	-0.989	0.008	-0.865	0.001	-0.865	0.001
TCARI/OSAVI	-0.956	0.000	-0.862	0.001	-0.862	0.001
MCARI	-0.990	0.000	-0.885	0.000	-0.859	0.001
$ANMB_{700\text{-}800}$	-0.995	0.000	-0.847	0.001	-0.848	0.001

*Pearson correlation coefficient, ** significance within the confidence interval of 0.95.

Results on the significance level and correlation coefficients in table 10 suggest that all the tested optical indices have a strong correlation with the Ch_{a+b} content at the level of needles. The first case of the PROSPECT data had the highest Pearson correlation coefficient (0.96 – 0.99);

[8] The statistical software SPSS version 10.0 works with 5 decimal placements, meaning that these values were less then 0.000.

then it decreased in case of real data (0.86-0.88) and the lowest values were obtained in the third case (0.85-0.87). The conclusion of this analysis is that all the indices were responding similarly to the clear information as well as information influenced by the presence of lichen optical properties. This test proved proper selection of the optical indices used for this work. However the remaining question was; what is their performance at the level of the forest canopy.

Leaf reflectance signatures simulated by the PROSPECT model were also used to validate the sensitivity of the optical indices for changes in chlorophyll content. The results are depicted in figure 8, where the independently changing variable is the Ch_{a+b} content and the dependent variables are the different optical indices.

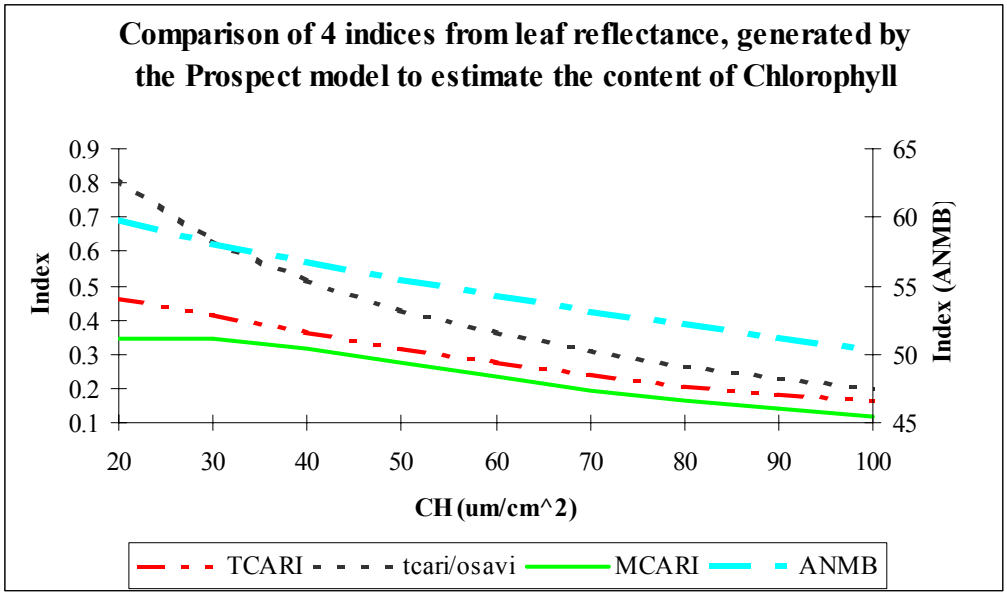

Figure 8. Sensitivity to Ch_{a+b} variability of 4 optical indices at needle level generated by the PROSPECT model.

As one can see the optical indices $ANMB_{700-800}$, TCARI and TCARI/OSAVI have a constantly decreasing trend with increase of the Ch_{a+b} content. This consistency expressed that there are no confounding variables for these indices, i.e. there is only one index value per Ch_{a+b} content. This is not the case for the MCARI index where almost similar values of 0.294 and 0.295, respectively, resulted from a chlorophyll content of 20 and 30 $\mu g/cm^2$. This behavior denotes a sensitivity limitation of MCARI at low pigment concentration, probably due to its response to non-photosynthetic leaf material (Haboudane et al., 2002). The lowest value of Ch_{a+b} content measured in the frame of this work was 28 $\mu g/cm^2$, so this confounding effect will probably not affect the performance of the MCARI index. The trends of the indices TCARI, TCARI/OSAVI and MCARI start flattening after Ch_{a+b} content of 80 $\mu g/cm^2$, which could indicate low sensitivity

of these indices to high chlorophyll values. Reflectance of the spectral bands used to compute these indices could get saturated by the high Ch_{a+b} content (see figure 9 for more explanation). The index $ANMB_{700-800}$ is not affected by this trend, which would indicate its high prediction suitability.

The slope of the reflectance differences between two successive contents of Ch_{a+b} was calculated based on the following formula, to investigate how the reflectance of spectral bands used in the indices connected to chlorophyll concentration behaves in terms of saturation:

$$\textbf{Slope} = \frac{(Y_2 - Y_1)}{(X_2 - X_1)} \qquad \textbf{(19)}$$

Where X represents the chlorophyll content and Y represent the percentage of reflectance. The slope coefficients of the reflectance of the four used spectral bands are plotted in figure 9 against the intervals of Ch_{a+b} concentration.

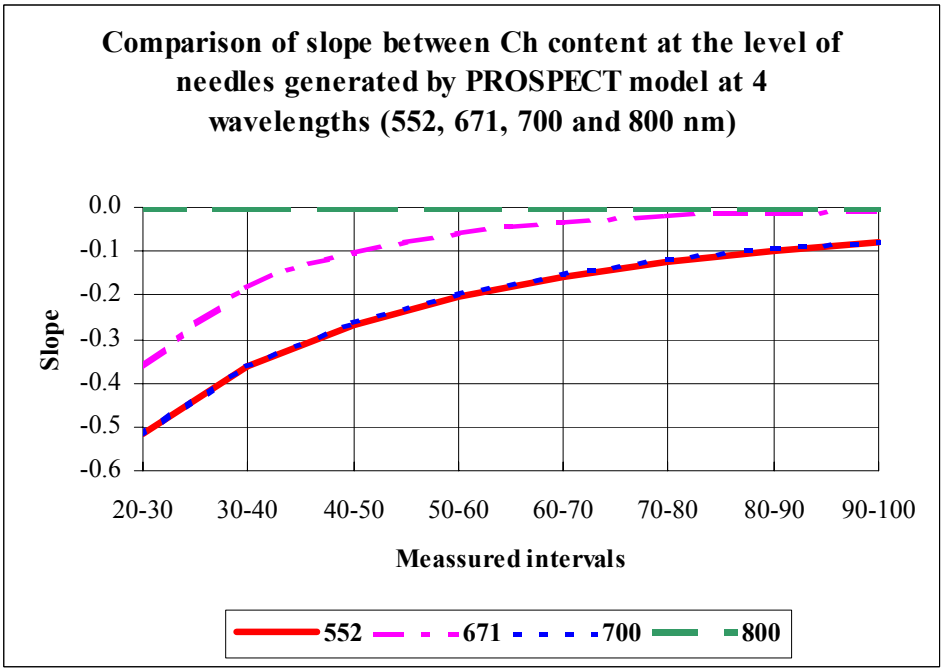

Figure 9. Comparison of slope between Ch_{a+b} content at needle level generated by PROSPECT in four spectral bands used by the optical indices.

The slope values computed from the reflectance of spectral bands 552 nm, 671 nm and 700 *n*m have quite similar tendencies, i.e. when the content of Ch_{a+b} increases the slope of reflectance differences decreases. The spectral region around a wavelength of 680 *n*m corresponds to the absorption peak of Ch_a and the region around 550 *n*m (green part) corresponds to the minimum chlorophyll absorption in the visible spectral domain (Haboudane et al., 2002). Reflectance of all

three bands, specially the band 671, is saturated at Ch_{a+b} concentrations greater than 80 µg/cm^2 (flat line of their graphs means no variability – see figure 9). Based on this information, it can be stated that these indices will not predict values of chlorophyll concentration greater than 80 µg/cm^2 in a consistent manner.

The preliminary results at the leaf level indicate that the indices TCARI and TCARI/OSAVI would estimate values between 20 and 80 µg/cm^2 in an accurate way. MCARI should perform well between 30 and 80 µg/cm^2 and $ANMB_{700-800}$ is expected to determine well values between 20 and 100 µg/cm^2. These results are valid only at the leaf level; therefore the indices have to be evaluated at canopy level to determine their performance in retrieving Ch_{a+b} values from crowns of a forest stands.

4.5. Performance of selected optical indices at the canopy level

The methodology of empiricall scaling-up is based on a relationship established between the canopy vegetation optical indices and the content of chlorophyll. The required statistical relation was carried out using the BRDF database, where the LAI, Ch_{a+b} and % of canopy closure were free variables (see section 3.10). The regressions and their determination coefficients can be seen in appendix 6. In general, regressions of all the indices have a very high r^2 (0.93- 0.99), meaning that indices should be able to predict well the content of chlorophyll at the canopy level. Similar results were obtained by Haboudane et al. (2002) where the coefficient of determination exceeded 0.98 for the TCARI/OSAVI ratio. In their work the logarithmic scaling-up relationship was chosen because it has been found as a consistent chlorophyll content estimator. Also results of our study showed the logarithmic regression to be the most appropriate function to predict the content of chlorophyll from the optical indices. As examples the indices TCARI and MCARI are shown in figure 10.

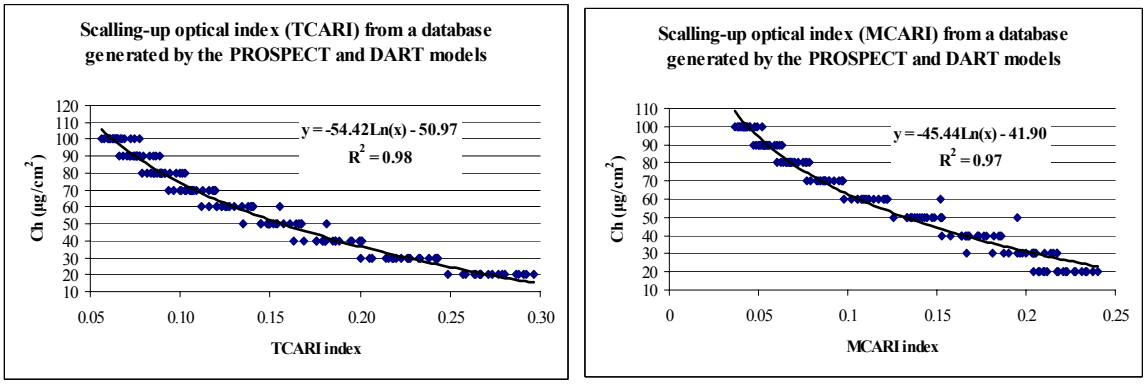

Figure 10. Logarithmic relation between chlorophyll content and the optical ratios TCARI and MCARI at the level of a canopy generated by the PROSPECT and DART models.

4.6. Evaluation of the chlorophyll prediction methods using a simulated hyperspectral image of a forest stands

Three scaling-up methods (vegetation optical indices, merit function and neural network approach) were used to estimate the content of chlorophyll from a simulated hyperspectral image of the forest stand. Their performance was evaluated for hyperspectral images of three different scenarios: (1) "pure" spruce canopy without any side effect, (2) canopy with the optical properties mixed with lichen optical properties at a ratio 1:5, and (3) canopy with 20% plus zero-mean Gaussian noise generated for a SNR of 5. The results are presented in tables 11, 12 and 13.

4.6.1. Method of the vegetation optical indices applied to scaled-up spectral bands

The indices TCARI, TCARI/OSAVI and MCARI were able to successfully estimate the chlorophyll content of the sample trees in case of scenarios 1 and 2 (see table 11). The level of correlation significance was lower than 0.05 meaning that predicted values are statistically very close to the measured ones. The scenario 1 shows better results compared to scenario 2, meaning that the influence of lichens could affect the results of this method, if their presence through the canopy will increase. The presence of noise and lichen optical properties together, scenario 3, affected strongly the performance of all the indices. There none of the used indices were able to predict the Ch_{a+b} content properly in this scenario. The significance level for the MCARI index was close to the 5% of α- level, but still making this correlation not statistically significance.

Table 11. Scaling-up method of the vegetation optical indices.

	Scenario 1 (true data)		Scenario 2 (lichens)		Scenario 3 (lichens + noise)	
Optical indices	R*	Sig.**	R	Sig.	R	Sig.
TCARI	0.791	0.001	0.735	0.004	0.391	0.186
TCARI / OSAVI	0.774	0.002	0.726	0.005	0.431	0.142
MCARI	0.889	0.001	0.831	0.001	0.524	0.066
$ANMB_{700-800}$	0.440	0.132	0.014	0.963	-0.274	0.364

The independent variable was the Ch_{a+b} content measured and the dependent variable the Ch_{a+b} content estimated by the indices, *Pearson correlation, **significant within α- confidence interval of 0.95.

The Chlorophyll Absorption in Reflectance Index (CARI) (Kim et al., 1994) is the original index from which the indices TCARI, TCARI/OSAVI and MCARI were generated. MCARI tries to minimize the underlying soil reflectance and the canopy non-photosynthetic material by adding the ratio (Ref_{700} / Ref_{670}). Nevertheless, this index is still sensitive to background reflectance being difficult to interpret at low values of LAI (Daughtry et al., 2000) and Ch_{a+b} (Haboudane et

al., 2002). TCARI tries to counteract the effects of the background (soil and non-photosynthetic materials) by using the ratio (Ref_{700} / Ref_{670}) influencing just the difference ($Ref_{700} - Ref_{550}$). Despite this improvement, the index is still sensitive to the underlying background reflectance properties, particularly in case of low LAI values (Rondeaux et al., 1996). To compensate for this problem Haboudane et al. (2002) proposed to combine the TCARI index with a soil line vegetation index (OSAVI). This ratio makes accurate predictions of crop chlorophyll content, and it has been shown to be relatively insensitive to canopy cover variations, even with low LAI values. These modifications made to the CARI index tried to reduce the effect of the soil background and non-photosynthetic material, which is not the case of our work. At the time of this study the DART model was not able to simulate the branches of first order inside the canopy, which means that low LAI of the tree crowns only allowed increase of the background (understorey) and inner trunk influence. The background was covered mainly by grasses, so the effect of bare soil on the canopy reflectance was not present. These facts could explain why MCARI had the best performance compare to the other indices. It is important to remember that only the sunlit pixels were used to obtain the optical properties of the trees of interest (between 4 and 6 pixels per crown depending on its diameter). This selection also decreased the background effect and can explain in some extend the performance of this index. The new version of the DART is supposed be able to model directly the branches of first order and wood turbid cells inside the canopy. Because the spectral signatures of raw bark have quite similar optical properties compare to the bare soil, the low values of crown LAI could imitate bare soil as a background inside the crown. It would be interesting to explore the effect of branches and woody twigs in case of low LAI on the performance of the optical indices.

The optical properties of the "sample" trees of interest in scenario 2 were affected by the presence of most common species of lichen in a constant way. In figure 11 a comparison between the optical properties of scenario 1 and scenario 2 at canopy level are given. The presence of lichens increased the reflectance in the visible part of the spectrum and decreased the reflectance in the NIR. These changes didn't affect the performance of optical indices up-scaling retrieval methods. The ratios of bands within the optical indices were able to eliminate the effect of the presence of lichens. A comparison of the average index values from scenario 1 and 2 was performed to evaluate the robustness of the optical indices. The TCARI index was minimally affected by the presence of lichens; it was able to compensate for this kind of additional information. Making a comparison of this index obtained from scenario 1 and scenario 2, we did not find any significant difference (see table inside figure 11).

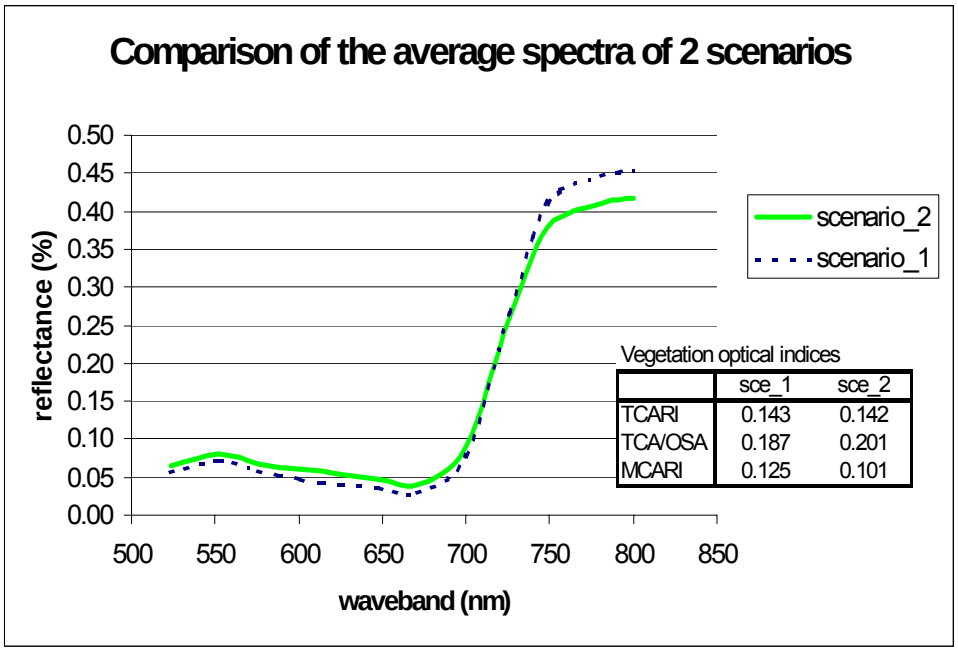

Figure 11. Average canopy spectral signatures for scenario 1 and 2.

The modifications made to TCARI during the transformation from MCARI (the ratio Ref_{700} / Ref_{670} influences only the difference $Ref_{700} - Ref_{550}$) could be the reason why this optical index was able to compensate for the presence of lichens. Values of the TCARI/OSAVI ratio were driven by the denominator (OSAVI index). The reduction of the reflectance at the NIR plateau decreased the OSAVI mean value from 0.77 to 0.71, which caused an increase in predicted chlorophyll content.

The addition of the noise to scenario 2 resulted in an image with a SNR of 5, which can be considered as a very noisy data. None of the chosen optical indices was able to predict accurately the content of Ch_{a+b} for scenario 3. This might be explained by means of the data creation. The zero-mean noise was distributed randomly per spectral band in the real scenes, but its effect was not introduced when the BRDF database was generated. The optical indices were not able to compensate for the noise and the predicting capability of the statistical equations decreased. A graphical comparison of canopy spectral signatures of all three scenarios for two selected trees is given in figure 12 in order to observe the variability introduced into the spectral signatures by the randomly generated noise.

The optical index $ANMB_{700-800}$ was not able to predict the Ch_{a+b} content at the canopy level. However, it was expected to perform well based on the results obtained at the needle level. This discrepancy could be related to the low Pearson correlation (see appendix 7) obtained for the

optical band at 749 *n*m and the Ch_{a+b} content at the canopy level. Due to the low number of bands available to calculate this index, this band at 749 *n*m was always selected as the maximum band depth (MBD), so its value was negatively influential on this index. It's also worth to mention that there was a positive correlation influence of the dry matter (C_m) content on this index at the needle level, as the coefficient of determination between C_m and Ch_{a+b} was 0.95 (see appendix 9). This can be explained by the fact that the NIR reflectance is affected by the amount of transitions between cell walls and air intercellular spaces in the leaf tissue, which is related to the dry matter content; so an increase in dry matter will increase also the reflectance at the NIR plateau (Lillesand and Kieffer, 2000). Dry matter concentration affects directly the area under the continuum-removed inverted reflectance curve (AUC) forcing it to have a high correlation with the Ch_{a+b} content. This relation could be the reason why the high performance of this index at the level of needles.

4.6.2. Methods of a merit function applied to scaled-up spectral bands

In the first run all 12 bands were used to determine the capability of a merit function to predict the Ch_{a+b} content. The resulting prediction was assessed to be inaccurate, because the significance α- level of regression was higher than 0.05 (see table 12), which means that predicted and measured values were statistically different. Based on this finding a Pearson correlation was used between reflectance of all spectral bands and the chlorophyll content within the BRDF reference database (see appendix 7). Spectral bands with correlation coefficient less than 0.60 were rejected for the next analysis. The second run of the merit function up-scaling, performed on the new 9 band dataset, increased the accuracy of the result, and the correlation significance was found to be significant. However the merit function approach was not able to predict properly the content of Ch_{a+b} in scenario 2, because the method did not contain any corrective mechanism for the presence of lichen optical properties. The capability of this method in frame of the noisy scenario 3 was reduced even more.

Table 12. Evaluation of the scaling-up method using merit function.

Bands use in	Scenario 1 (real data)		Scenario 2 (lichens)		Scenario 3 (Lichens + noise)	
calculation	R*	Sig.**	R	Sig.	R	Sig.
1 till 12	0.492	0.088	0.369	0.215	0.105	0.734
1 till 9	0.674	0.011	0.522	0.067	0.148	0.629

The independent variable was the Ch_{a+b} content measured and the dependent variable the Ch_{a+b} content estimated by the merit function, *Pearson correlation, ** significance within a confidence interval of 0.95.

The use of the merit function was significantly affected by the set-up used to build up the BRDF database. The generated BRDF database varied only in the content of Ch_{a+b}, LAI and % of canopy closure. The effect of lichens and noise presence was not added, hence minimizing the cost function, looking for the smallest RMSE between the spectral signature of the simulated scenario and signatures of the BRDF database, failed to estimate correctly the chlorophyll amount. This was not the case of scenario 1, where the BRDF database contained all the required information to make the right predictions.

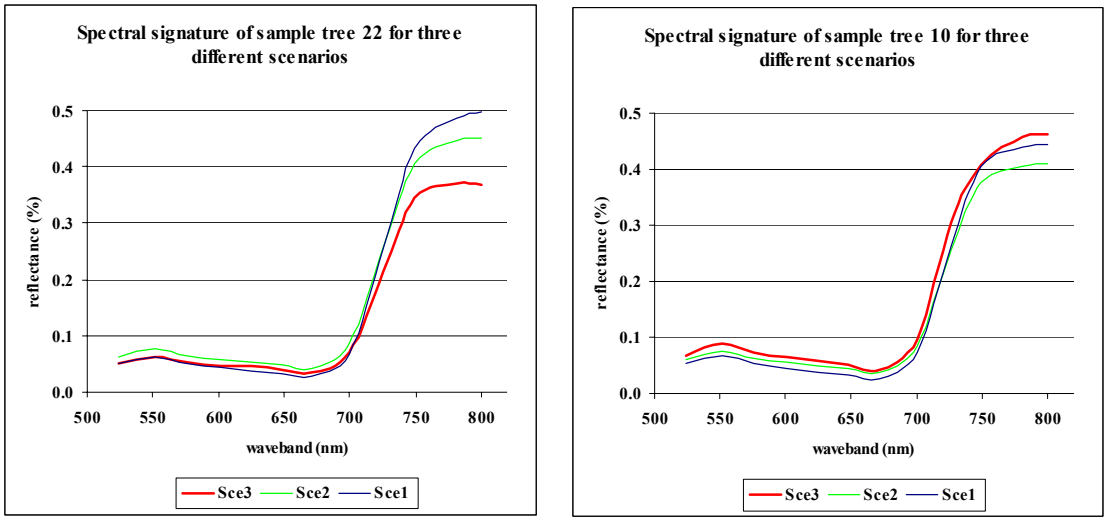

Figure 12. Spectral signatures of two Norway spruce crowns for all three considered scenarios.

The spectral signatures of two selected spruce crowns for all three scenarios are plotted in figure 12. As one can see the spectral signatures of the second scenario have an expected pattern when compared to the scenario l, i.e. increase of reflectance in the visible part and decrease in the NIR. The spectral signature of scenario 3 shows a high variability within wavelengths, i.e. the changes in reflectance are irregular. Therefore, the discrepancy in prediction by the merit function approach is very high. To compensate such a non-systematic variability is difficult and needs a more sophisticated algorithm.

An additional factor affecting negatively the accuracy of the merit function estimation was the minimal chlorophyll content increment of 10 $\mu g/cm^2$ introduced for the BRDF database creation. These constrain results in capability of the merit functions to predict only rounded Ch_{a+b} values (e.g. 40 or 50 $\mu g/cm^2$, but never 45 $\mu g/cm^2$).

4.6.3. Methods of neural network applied to scaled-up spectral bands

Both neural networks (NN) set-ups, based on cascade propagation, were able to predict accurately the Ch_{a+b} content for scenarios 1 and 2 with the statistical significance level lower than 0.05 (see table 13). In case of scenario 3 only the setup with 5% error introduced into the training dataset was able to estimate Ch_{a+b} precisely. It is very important to stress, that this was the only method able to have a significant correlation and proper chlorophyll prediction for the noisy scenario 3.

Table 13. Evaluation of the scaling-up method using a neural network (cascade propagation).

Neural network set-up		Scenario 1 (real data)		Scenario 2 (lichens)		Scenario 3 (Lichens + noise)	
Training	Test	R*	Sig.**	R	Sig.	R	Sig.
Database[9]+ 5% e	Database	0.713	0.006	0.834	0.001	0.715	0.006
Database+ 5% e + LAI	Database + LAI	0.650	0.016	0.771	0.002	0.358	0.230

The independent variable was the Ch_{a+b} content measured and dependent variables Ch_{a+b} content estimated by neural networks, *Pearson correlation, ** significance within confidence interval of 0.95.

The tendency of the previous methods was always a decrease in their performance when the disturbing effects were introduced. This was not the case for the neural network up-scaling approach. The best result was obtained for scenario 2, which could be explained by establishment of the NN. A +/- 5% error was added to the training database to increase the robustness of the neural network and to decrease the inner correlation between the reflectance values of training and testing sets. The system was learned on this information and the resulting NN was evaluated on a testing set (database without +/- 5% error). The spectral signatures of the 13 trees in scenario 1 were not affected by any disturbing factor, so the performance of neural networks might be expected to be lower compared to scenario 2, under assumption that the effect of lichen presence is equal to the 5% error added to the NN training database. This is the most probable explanation, why the NN approach performed better in case of scenario 2 than scenario 1. Also in scenario 3 the NN method was able to compensate for the extra added random noise, but not so efficiently as in scenario 2.

The addition of extra information like LAI to the training set and testing set didn't improve the performance of this method. All the Ch_{a+b} predictive results from this set-up were lower

[9] The database is conformed of the 9 spectral bands selected earlier during the merit function method.

compared to the one that didn't contain the LAI. This is explained by the low Pearson correlation between LAI and chlorophyll content (R = 0.29), so we conclude that the addition of extra structural information decreased the performance of the neural network.

To explain the performance of neural networks is very difficult, because they enable to relate a given set of input variables to a set of output variables, irrespective to any known functional relationship between input and output, providing an implicit relationship existing between these sets (Combal et al., 2002). The NN method does the learning and testing of the data and finally gives you an output. This process can be considered as a kind of "black box" procedure where something comes in and something comes out, but principles behind the results are unknown. In case of this study the learning process benefits from the additional of noise (+/- 5% error), but this is not a general rule and it might not be valid for another data set.

4.7. Comparison of the chlorophyll content retrieving approaches

Based on the findings of the previous sections we can summarize that three optical indices and two neural network set-ups were capable to predict suitably the chlorophyll content in scenarios 1 and 2. In case of scenario 3 only one method of the neural network retrieved correctly the content of Ch_{a+b}. The purpose of this study was to determine the best performing chlorophyll retrieving approach, thus a comparison of these methods was carried out. The predicting capability was measured by means of the RMSE (prediction - measured) and the determination coefficient of a linear regression. The results are described in table 14.

Table 14. Comparison of the best performing methods to estimate the content of Ch_{a+b}.

	Scenario 1 (true data)			Scenario 2 (lichen)			Scenario 3 (lichen + noise)		
Methods	Mean*	RMSE**	r^{2***}	Mean	RMSE	r^2	Mean	RMSE	r^2
Scaling-up TCARI	56.13	13.52	0.63	56.15	14.50	0.54	60.80	18.36	0.15
Scaling-up TCARI/OSAVI	57.99	**12.84**	0.60	54.09	15.96	0.53	56.95	18.23	0.19
Scaling-up MCARI	53.59	13.30	0.79	63.08	**10.06**	0.69	66.92	16.41	0.28
NN Database+5%*e*	61.89	13.97	0.51	69.91	11.69	0.70	71.08	**15.99**	0.52
NN Database+5%*e* +LAI	60.13	13.91	0.42	70.13	14.01	0.59	63.87	23.82	0.13

* Is the average Ch_{a+b} content of the predicted values, ** RMSE (root mean square error) is the difference between the measured and predictive value of chlorophyll *** is coefficient of determination (linear regression of predicted and measured Ch_{a+b} content). The average measured Ch_{a+b} content was 64.21 $\mu g/cm^2$.

The highest acceptable RMSE between retrieved and measured Ch_{a+b} was set to be 15 μg/cm^2, which is a statistically proved difference in chlorophyll concentration of the needles between spruce trees of RN and RT stress categories. The five tested methods were able to meet this limit for scenario 1, only four methods for scenario 2, and none of them succeeded to stay below this limit in case of scenario 3. By analyzing the results from table 14, up-scaling of the vegetation optical index TCARI/OSAVI is the best method to estimate the content of Ch_{a+b} in scenario 1. For scenario 2, the index MCARI is the best method to estimate the Ch_{a+b} content. Finally up-scaled neural network (database +/- 5%*e*) appeared to be the best working method in scenario 3.

From a first sight the up-scaling of the vegetation optical index MCARI seems to have the best performance in general. It was the second best method for the scenario 1, the best one for scenario 2 and the second best method for the scenario 3, again. The index MCARI showed some inconsistency in the prediction of the chlorophyll values. The average retrieved chlorophyll estimation for scenario 1 was 53.59 μg/cm^2, but for scenario 2 it was increased up to 63.08 μg/cm^2, which suggests the influence of the lichen thalluses presence. The TCARI is likely more robust optical index, because it presented almost no change in predicted Ch_{a+b} values between scenarios 1 and 2. This could be related to the improvements introduced into this index for a soil and non-photosynthetic material compensation. As one can see in table 14, the predicting capability of the MCARI index was increased by the "beneficial" effect of lichen appearance, due to the reflectance increase of all the spectral bands used to calculate this index. Based on this analysis it is worth to mention that if the percentage of lichen occurrence would increase even more, then the prediction done by MCARI index will probably overestimate the chlorophyll content.

The up-scaling methods based on the neural networks performed well for scenarios 2 and 3. Because of the MCARI index inconsistency in robustness, we can state that the NN up-scaled approach (database +/- 5%*e*) was the best performing method in general. For scenario 1 and 2 its RMSE was less than 15 μg/cm^2, this was the maximum tolerance value. The RMSE of scenario 3 exceeded this limit only very slightly (about 1 μg/cm^2). To achieve a real high spatial resolution hyperspectral image free of any noise (scenario 1) is practically impossible, so probably the scenarios 2 and 3 are more suitable and important to draw the final conclusion on the performance of the tested chlorophyll retrieving methods.

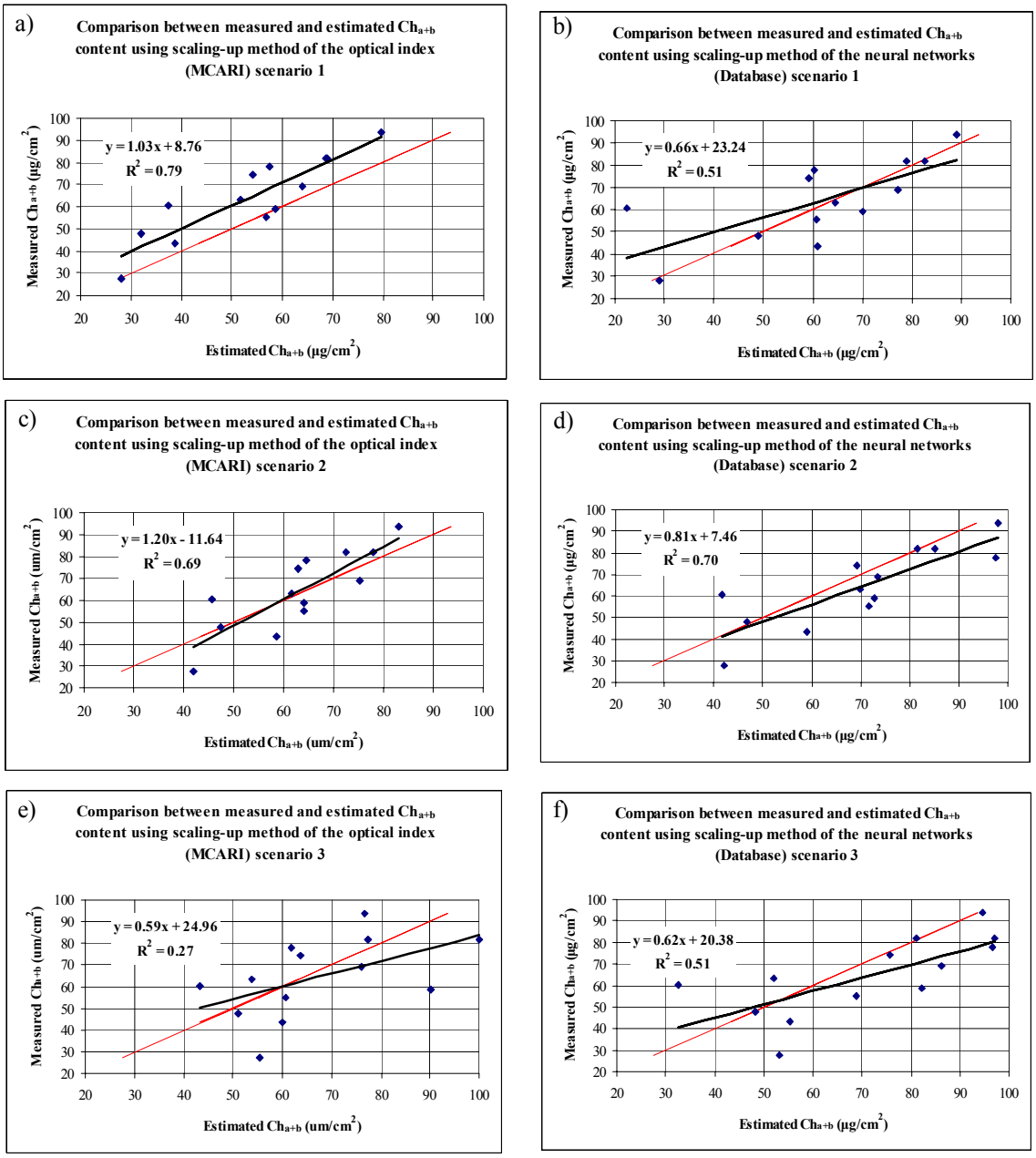

Figure 13. Comparison between measured and retrieved Ch_{a+b} content by means of used up-scaling methods.

Figure 13 shows the regressions between chlorophyll content estimated by the MCARI index and neural networks (database +/- 5% error), which turned out to be the best performing methods. The regression graphs of the other methods are described in the appendix 13. A detailed analysis was performed on these two methods to corroborate their performance by removing the most significant outlying value. The neural network approach is strongly affected by the outliers (see figure 13b) especially in scenario # 1 were the RMSE decreased from 13.97 µg/cm^2 of chlorophyll to 9.54 µg/cm^2 and the r^2 increased from 0.51 to 0.72. This indicates how strong was

the effect of this one value on the predicting capability of the NN method. We did not observe such a strong influence, caused by one outlier on NN approach results of the rest of the scenarios (RMSE decreased only by 1 μg/cm^2). For the optical index MCARI the effect of removing one outlier was not so influential it reduced the RMSE only by 1.5-0.5 μg/cm^2 in all the different scenarios. All these achievements are underlying the neural network method (database +/- 5% error) as the best performing approach within all the scenarios.

Zarco-Tejada et al., 2002 carried out a study with aims and methodology comparable with our present work. The chlorophyll amount was estimated from crown sunlit pixels of an airborne hyperspectral image using a merit function of the optical index Ref_{750} / Ref_{710}. Their results showed a lower coefficient of determination (r^2= 0.40) between the measured and estimated Ch_{a+b} concentration. On the other hand their RMSE for predicted and measured chlorophyll content ranging between 26.8 and 56.8 μg/cm^2 was only 8.1 μg/cm^2. Our best performing approach, NN up-scaling, had more significant coefficient of determination, but the RMSE was almost two times higher compared to their findings. The potential explanations of this phenomenon might be i) a low number of sample trees used in our work, and ii) a high variability of the sample crowns in Ch_{a+b} content. However, taking out one most significant outlying crown from the retrieval procedure forced the RMSE to drop down on the value of 9.54 μg/cm^2, which is already comparable with their results.

5. Conclusions and recommendations

The objective of this study was to contribute to the estimation of stress biochemical indicators of Norway spruce crowns by generating knowledge on the best performing method to determine the chlorophyll content from hyperspectral images of high spatial resolution. Three different scenarios were simulated, using the DART radiative transfer model, and later analyzed to solve the defined objective concerning the best performing method for chlorophyll content retrieval. Based on the obtained findings conclusions are:

1) For the simulated hyperspectral image of scenario 1 (no disturbing factor present) all three tested methodological approaches of up-scaling leaf optical properties to the level of the canopy were able to predict in an accurate way the chlorophyll content. The used up-scaling methods were: i) optical indices TCARI, TCARI/OSAVI, and MCARI, ii) Merit function for 9 spectral bands, and iii) neural networks (database and database + LAI). All methods showed a RMSE in chlorophyll prediction less than 15 μg/cm2, which was the maximum limit of tolerance. The best performance was obtained by the index TCARI/OSAVI.
2) In scenario 2 (presence of lichen optical properties in the canopy by a proportion of 20%), two general methods were able to predict accurately the chlorophyll content. The optical indices (TCARI and MCARI) and the neural networks approaches (database and database + LAI) had a RMSE less than 15 μg/cm2. However, the optical index MCARI seems to be influenced by the presence of lichen. Based on this the neural network (database +/- 5% error) approach was chosen as the best performing method of this scenario is.
3) In scenario 3 (image with SNR equal to 5 and presence of lichen by a 20% share on the crown optical properties) only one method was able to estimate correctly the chlorophyll content. The neural network (database) approach applied on up-scaled spectral bands produced the RMSE between estimated and measured chlorophyll concentration about 16 $\mu g/cm^2$, which is slightly higher than the required limit of 15 $\mu g/cm^2$. It is expected that the RMSE value would decrease below the defined limit with higher number of sample trees, and it was decreased by removing one significant outlier from the analysis.
4) The setup of the referential BRDF database is a crucial factor in the performance of the chlorophyll retrieving methods. The negative effect of not considering the lichens and noise presence in the BRDF database was discovered for the performance of the merit function approach. Consequently, this method wasn't able to perform well under scenarios 2 and 3. The used PROSPECT input parameters N, C_w and C_m were kept constantly fixed, due to the

time constrains of the BRDF database creation. This caused their systematic under and/or overestimation (see appendix 9). The influence of this potential negative factor was not directly investigated, but there is a strong recommendation for the next studies to let these parameters varying.

Based on the obtained results we can generally conclude that the best performing method to retrieve the chlorophyll content over a spruce forest stand simulated by the DART model was the scaling-up approach of the neural network (cascade propagation network generated from BRDF database with +/- 5% error). From the three different scenarios, of varying conditions of interest, the neural network approach performed well over the scenario 2 (lichen presence) and the best over scenario 3 (noise + lichen presence). In case of scenario 1 (no disturbing factor) it was not the best method when all the samples were consider, but when removing one outlier the RMSE decreased to 9.54 $\mu g/cm^2$, which was the lowest one. It is necessary to stress that these results need further testing, because they were carried out using only 13 sample of Norway spruce trees. Furthermore, the conclusions are based only on the data simulated by the DART radiative transfer model. Therefore, they should be verified by a next study using a real hyperspectral image of high spatial resolution obtained from a complex airborne/field campaign over the Norway spruce forest stand.

6. References

Bruniquel-Pinel, V., and J. P. Gastellu-Etchegorry, 1998, Sensitivity Of Texture Of High Resolution Images Of Forest To Biophysical And Acquisition Parameters: Remote Sensing of Environment, v. 65, p. 61-85.

Chelle, M., 1997, Developpement D'un Modele De Radiosite Mixte Pour Simuler La Distribution Du Rayonnement Dans Les Couverts Vegetaux. Institut De Formation Superieure En Infomratique Et Telecommunication, Universite de Rennes, Rennes, 161 p.

Chen, J. M., 1996, Optically-Based Methods For Measuring Seasonal Variation Of Leaf Area Index In Boreal Conifer Stands: Agriculture and Forest Meteorology, v. 80, p. 135-163.

Combal, B., F. Baret, M. Weiss, A. Trubuil, D. Mace, A. Pragnere, R. Myneni, Y. Knyazikin, and L. Wang, 2002, Retrieval Of Canopy Biophysical Variables From Bi-Directional Reflectance Using Prior Information To Solve The Ill-Posed Inverse Problem: Remote Sensing of Environment, v. 84, p. 1-15.

Combal, B., Baret, F., Weiss, M., Trubuil, A., Mace, D., Pragnere, A., Myneni, R., Knyazikin, Y. and L. Wang, 2002, Retrieval Of Canopy Biophysical Variables From Bi-Directional Reflectance Using Prior Information To Solve The Ill-Posed Inverse Problem: Remote Sensing of Environment, v. 84, p. 1-15.

Cutini, A., G. Matteucci, and G. S. Mugnozza, 1997, Estimation Of Leaf Area Index With The Li-Cor LAI 2000 In Deciduous Forests: Forest Ecology and Management, v. 105, p. 55-65.

Daughtry, C. S. T., L. L. Biehl, and K. J. A. Ransom, 1989, New Technique To Measure The Spectral Properties Of Conifer Needles: Remote Sensing of Environment, v. 27, p. 81-91.

Daughtry, C. S. T., C. L. Walthall, and M. S. Kim, 2000, Estimating Corn Leaf Chlorophyll Concentration From Leaf And Canopy Reflectance: Remote Sensing Environment, v. 74, p. 229-239.

Demarez, V., and J. P. Gastellu-Etchegorry, 2000, A Modeling Approach For Studying Chlorophyll Content: Remote Sensing of Environment, v. 71, p. 226-238.

Fisher, B., Perkins, S., Walker A. and E. Wolfart., 1994, Noise generation: http://www.cee.hw.ac.uk/hipr/html/noise.html, Edinburgh, Department of Artificial Intelligence University of Edinburgh.

Frankis, M. P., 1999, http://www.botanik.uni-bonn.de/conifers/pi/pic/abies.htm.

Garcia-Haro, F. J., and S. Sommer, 2001, A Fast Canopy Reflectance Model To Simulate Realistic Remote Sensing Scenarios: Remote Sensing of Environment, v. 84, p. 205-227.

Gascon, F., 2001, Modelisation Physique D'images De Teledetection Optique: Dissertation thesis, Toulouse, Toulouse, 137 p.

Gastellu-Etchegorry, J. O., V. Demarez, Pinel, V., and F. Zagolsky, 1996, Modeling Radiative Transfer In Heterogeneous 3-D Vegetation Canopies: Remote Sensing Environment, v. 58, p. 131-156.

Gastellu-Etchegorry, J. P., F. Gascon, and P. Esteve, 2003, An Interpolation Procedure For Generalizing A Look-Up Table Inversion Mothod: Remote Sensing Environment, v. 87, p. 55-71.

Gastellu-Etchegorry, J. P., E. Martin, and F. Gascon, 2004, DART: A 3D Model For Simulating Satellite Images And Studying Surface Radiation Budget: International Journal of Remote Sensing, v. 25, p. 73-96.

Gitelson, A. A., and M. N. Merzlyak, 1997, Remote Estimation Of Chlorophyll Content In Higher Plant Leaves: International Journal of Remote Sensing, v. 18, p. 2691-2697.

Govaerts, Y., and M. M. Verstraete, 1998, Raytran: A Monte Carlo Ray Tracing Model To Compute Light Scattering In Three-Dimensional Heterogeneous Media: IEEE Transaction on Geoscience and Remote Sensing, v. 36, p. 493-505.

Gower, S. T., and J. M. Norman, 1990, Rapid Estimation Of Leaf Area Index In Forests Using Li-Cor LAI 2000: Ecology, v. 72, p. 1896-1900.
Grace, J. C., 1987, Theoretical Ratio Between "One-Side" And Total Surface Area For Pine Needles: N.Z.J. Forestry Science, v. 17, p. 292-296.
Haboudane, D., J. R. Miller, N. Temblay, P. J. Zarco-Tejada, and L. Dextraze, 2002, Integrated Narrow-Band Vegetation Indices For Prediction Of Crop Chlorophyll Content For Application To Precision Agriculture: Remote Sensing of Environment, v. 81, p. 416-426.
Huemmrich, K. F., 2001, The Geosail Model: A Simple Addition To The SAIL Model To Describe Discontinuous Canopy Reflectance: Remote Sensing Environment, v. 75, p. 423-431.
IFER, 2002, http://www.ifer.cz/en/products/fieldmap/index.php.
Jacquemoud, S., C. Bacour, H. Poilve, and J. P. Frangi, 2000, Comparison Of Four Radiative Transfer Models To Simulate Plant Canopies Reflectance: Direct And Inverse Mode: Remote Sensing Environment, v. 74, p. 471-481.
Jacquemoud, S., and F. Baret, 1990, PROSPECT: A Model Of Leaf Optical Properties Spectra: Remote Sensing Environment, v. 34, p. 75-91.
Jasinski, M. F., 1990, Functional Relation Among Subpixel Canopy Cover, Ground Shadow And Illuminated Ground At Large Sampling Scales: Society of photo optical instrumentation engineers.
Johnson, L. F., C. A. Hlavka, and D. L. Peterson, 1994, Multivariate Analysis Of Aviris Data For Canopy Biochemical Estimation Along The Oregon Transect: Remote Sensing Environment, v. 47, p. 216-230.
Kim, M. S., C. S. T. Daughtry, E. W. Chappelle, J. E. McMurtrey III, and C. L. Walthall, 1994, The Use Of High Spectral Resolution Bands For Estimating Absorbed Photosynthetically Active Radiation: 6th Symposium on Physical Measurements and Signatures in Remote Sensing.
Kimes, D. S., and J. A. Kirchner, 1982, Radiative Transfer Model For Heterogeneous 3-D Scenes: Appl. Opt., v. 21, p. 4119-4129.
Lillesand, T. M., and R. W. Kieffer, 2000, Remote Sensing And Image Interpretation: New York, John Wiley & Sons, Inc., 724 p.
Logical-designs, 1996, Thinkspro Users Guide, La Jolla, p. 370.
Malenovsky, Z., 2003, Area Normalized To Maximal Band Depth Between 700 And 800 Nm ($ANMB_{700\text{-}800}$), Personal communication.
North, P. R. J., 1996, Three-Dimensional Forest Light Interaction Model Using A Monte Carlo Method: IEEE Transactions on Geoscience and Remote Sensing, v. 34, p. 946-956.
Pinty, B., N. Gabron, J. L. Wildowsky, S. A. W. Gerstl, M. M. Vertraete, M. Antunes, C. Bacour, F. Gascon, J. P. Gatellu-Etchegorry, S. Jacquemoud, P. North, W. Qin, and T. R., 2001, Radiation Transfer Model Intercomparison (RAMI) Exercise: Journal of Geophysical research, v. 106, p. 1937-1956.
Porra, R. J., W. A. Thompson, and P. E. Kriedeman, 1989, Determination Of Accurate Extinction Coefficient And Simultaneous Equations For Assaying Chlorophylls A And B Extracted With Four Different Solvents: Verification Of The Concentration Of Chlorophyll Standards By Atomic Absorption Spectroscopy: Biochimica and Biophysica Acta, v. 975, p. 384-394.
Rondeaux, G., M. Steven, and F. Baret, 1996, Optimization Of Soil-Adjusted Vegetation Indices: Remote Sensing Environment, v. 55, p. 95-107.
Thompsson, R. L., and N. S. Goel, 1998, Two Models For Rapidly Calculating Bidirectional Reflectance: photon spread (ps) model and statistical photon spread (sps) model.: Remote sensing reviews, v. 16, p. 157-207.
Ulrich, B., 1984, Process Hierarchy In Forest Ecosystem: An Integrative Ecosystem Theory. In Godbold, D., L., Huttermann, A. (Eds): Effects Of Acid Rain On Forest Processes: New York, Wiley-Liss, 353-397 p.

Verhoef, W., 1984, Light Scattering By Leaf Layers With Application To Canopy Reflectance Modelling: The SAIL Model: Remote Sensing Environment, v. 16, p. 25-141.
Welles, J. M., and J. M. Norman, 1991, Instrument For Indirect Measurement Of Canopy Architecture: Agronomy Journal, v. 83, p. 818-825.
Zarco Tejada, P., J. Miller, J. Harron, B. Hu, T. Noland, N. Goel, G. Mohammed, and P. Sampson, 2004, Needle Chlorophyll Content Estimation Through Model Inversion Using Hyperspectral Data From Boreal Conifer Forest Canopies: Remote Sensing Environment, v. 89, p. 189-199.
Zarco-Tejada, P., Miller, J., Noland, T., Mohammed, G and P. Sampson, 2001, Scaling-Up And Model Inversion Methods With Narrowband Optical Indices For Chlorophyll Content Estimation In Closed Forest Canopies With Hyperspectral Data: IEEE Transactions of Geoscience and Remote Sensing, v. 39, p. 1491-1506.

7. Appendices

Appendix 1. Distribution of the age classes of Norway spruces needles from two reactions to multiple stress.

Appendix 2. Clumping index within the shoot, needle-to-shoot area ratio $\gamma_{E.}$

Appendix 3. Element clumping index at scale larger than shoot $\Omega_{E.}$

Appendix 4. Clumping index (Ω) per functional part of Norway spruce.

Appendix 5. Statistical relationship between percentage of crown defoliation and Leaf area index.

Appendix 6. Determination coefficients of several regressions between optical indices and Ch_{a+b} content at canopy level generated by the PROSPECT and DART models.

Appendix 7. Pearson correlation coefficient between reflectance of the optical bands and Ch_{a+b} content at the canopy level.

Appendix 8. Functions of the leaf angel distribution (LAD) defined in the DART model.

Appendix 9. Comparison between measurements of Norway spruce needle biophysical parameters (leaf internal structure, dry matter content and water content) with the values used to simulate the hemispherical optical properties in the PROSPECT.

Appendix 10. Optical properties of representative elements used to create a realistic Norway spruce forest stand.

Appendix 11. Hyperspectral images simulated by the DART model, the RGB colour composition of investigated forest stands (scenario 1).

Appendix 12. Hyperspectral images simulated by the DART model, a RGB colour composition of the temporal research plot # 4 (scenario 2).

Appendix 13. Comparison between measured and retrieved Ch_{a+b} content using up-scaling methods (optical indices, merit functions and neural networks)

Appendix 1. Distribution of the age classes of Norway spruces needles from two reactions to multiple stress.

	Percentage of age classes of needles				
Tree id	C	C + 1	C + 2	C + older	C +2 + older
3001	12.27	30.66	19.70	37.37	57.07
3002	16.01	21.10	14.84	48.05	62.89
RN	**14.11**	**25.95**	**17.30**	**42.64**	**59.94**
3005	9.75	13.39	14.59	62.27	76.86
3006	14.75	13.08	11.78	60.39	72.17
RT	**11.76**	**13.27**	**13.46**	**61.51**	**74.97**

The information presented in the above table describes the volume weighted average of needle ages per stress classes.

Appendix 2. Clumping index within the shoot, needle-to-shoot area ratio γ_E.

		Measured projected area in cm^2 (10 shoots)			
Tree Type	Functional part	Needles	Shoots	Twigs	γ_E
RN	Juvenile	381.79	134.54	40.07	**3.14**
	Upper-production	310.50	152.29	33.80	**2.26**
	Lower-production	758.00	271.70	82.05	**3.09**
	Saturation	356.46	173.11	38.67	**2.28**
	Average	393.50	181.09	42.61	**2.41**
RT	Juvenile	672.95	252.17	69.26	**2.94**
	Upper-production	1365.61	529.90	136.84	**2.84**
	Lower-production	685.02	331.84	64.58	**2.26**
	Saturation	932.29	531.24	90.68	**1.93**
	Average	426.63	228.92	41.88	**2.05**

This information was obtained from the "destructive" sample trees where only 10 shoots per sample unit (SU) were analyzed.

Appendix 3. Element clumping index at scale larger than shoot Ω_E.

Tree Type	Functional part	Measured area in cm^2 (hole branch)			Ω_E
		Shoots	Projected branch	Wood	
RN	Juvenile	2680.77	1189.10	39.00	**0.44**
	Upper-production	4037.79	2972.74	120.58	**0.71**
	Lower-production	9288.02	11890.96	358.65	**1.23**
	Saturation	11132.67	15312.16	617.39	**1.30**
	Average	10271.15	13777.62	540.79	**1.27**
RT	Juvenile	3925.67	1593.42	47.85	**0.40**
	Upper-production	7217.34	5884.22	333.60	**0.78**
	Lower-production	12503.55	16071.38	638.18	**1.22**
	Saturation	22276.41	28438.11	1079.75	**1.22**
	Average	18544.11	22347.28	875.06	**1.15**

These measurements were obtained from the "destructive" sample trees. The projected branch area was estimated, based on a visual assessment. This information needs further knowledge to obtain more precise projected branch area. This parameter than can affect the outcome significantly.

Appendix 4. Clumping index (Ω) per functional part of Norway spruce.

Functional part	Level	Reaction to multiple stress		Average Ω
		Ω of RN	Ω of RT	
Juvenile	**1**	**0.14**	**0.14**	**0.14**
Production	**2**	**0.32**	**0.27**	**0.29**
	3	0.36	0.41	0.38
	4	**0.40**	**0.54**	**0.47**
Saturation	5	0.45	0.55	0.50
	6	0.50	0.60	0.55
	7	**0.57**	**0.63**	**0.60**
	8	0.57	0.63	0.60
	9	0.60	0.65	0.62
	10	0.65	0.70	0.67

The data was obtained from the "destructive" sample trees; the intermediate results are described in appendix 2 and 3. The values highlighted were the measured ones. It is worth to mention that the average per functional part was maintained. For the saturation part there was only one measurement, but 6 levels were made: level 7 and 8 are the averages and for the rest +/- 5% was added. In the production part the measured levels were 2 and 3 and an average of them was made to carry out level 3. The juvenile part is the percentage of measured clumping.

Appendix 5. Statistical relationship between percentage of crown defoliation and Leaf area index.

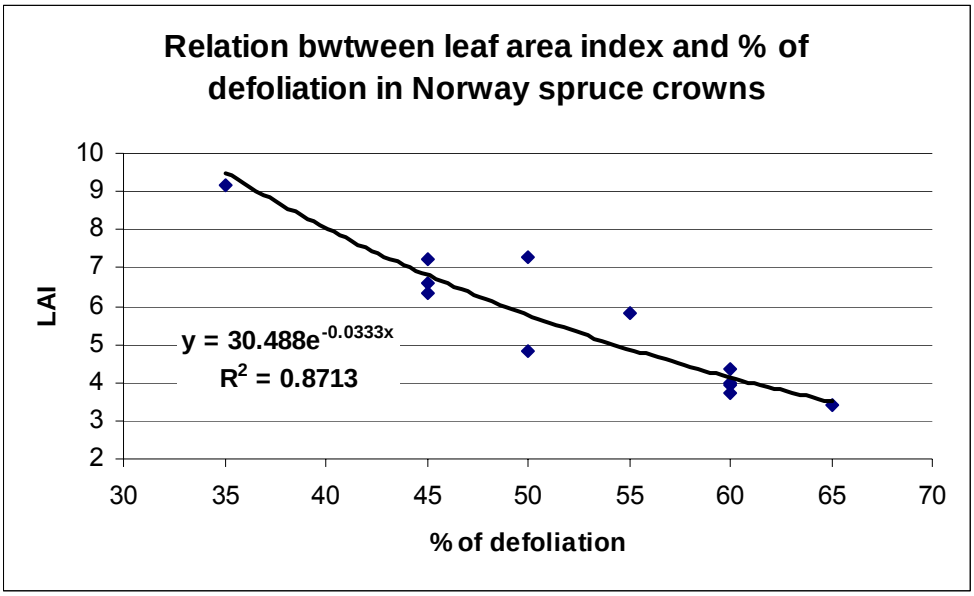

A regression between the L and the percentage of defoliation of the 13 trees of interest was performed. Only 11 trees were used in the analysis, the remaining crowns were excluded because they were considered as outliers.

Appendix 6. Determination coefficients of several regressions between optical indices and Ch_{a+b} content at canopy level generated by the PROSPECT and DART models.

Optical indices	Regression - determination coefficient			
	(Linear) r^2	(Polynomial 2nd order) r^2	(Exponential) r^2	(Log) r^2
TCARI	0.93	0.98	0.98	0.99
TCARI / OSAVI	0.89	0.97	0.97	0.97
MCARI	0.96	0.98	0.95	0.97
$ANMB_{700-800}$	0.93	0.94	0.95	0.93

The independent variable was the Ch_{a+b} content and the dependent variable was represented by the optical index. The 162 samples were used, generated by the PROSPECT (Ch content 20, 30, 40, 50, 60, 70, 80, 90, 100) and up-scaled by the DART (LAI, 2, 3, 4, 5, 7 and 9 and % scene coverage 35, 55 and 80).

Appendix 7. Pearson correlation coefficient between reflectance of the optical bands and Ch_{a+b} content at the canopy level.

Optical band (nm) wavelength	Database*	Trees**	Trees + Lichens**	Trees + Lichens + Noise**
524	-0.92	-0.43	-0.44	-0.16
552	-0.93	-0.55	-0.60	-0.33
576	-0.61	-0.45	-0.43	-0.22
601	-0.91	-0.38	-0.37	-0.10
625	-0.90	-0.25	-0.24	0.02
648	-0.88	-0.14	-0.11	0.09
671	-0.84	0.12	0.06	0.13
700	-0.93	-0.58	-0.50	-0.18
726	-0.88	-0.54	-0.48	-0.07
749	-0.23	0.05	-0.02	0.05
781	-0.07	0.32	0.26	0.26
800	-0.08	0.27	0.11	0.17

* All 162 samples were used to perform this correlation.

** Optical properties of 13 "sample" trees were used to perform this correlation.

Appendix 8. Functions of the leaf angel distribution (LAD) defined in the DART model.

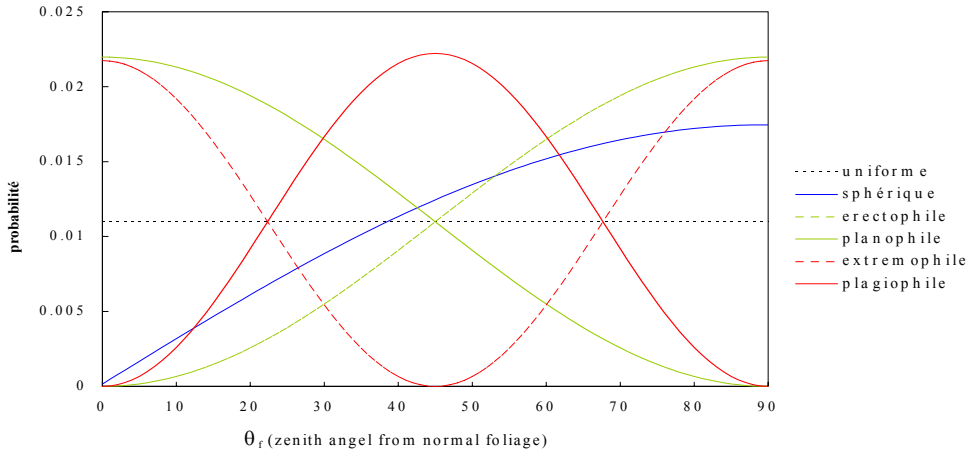

Referred to Gascon (2001)

Appendix 9. Comparison between measurements of Norway spruce needle biophysical parameters (leaf internal structure, dry matter content and water content) with the values used to simulate the hemispherical optical properties in the PROSPECT.

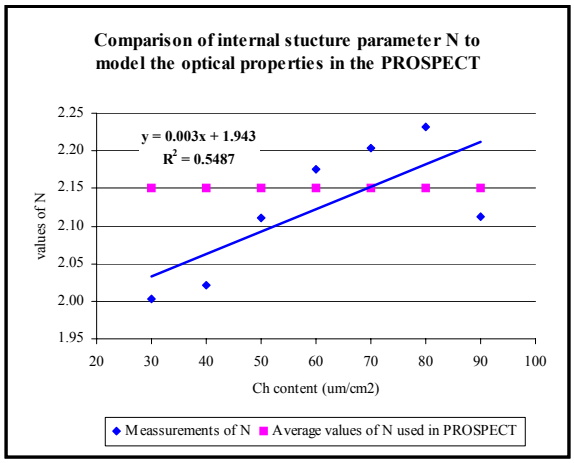

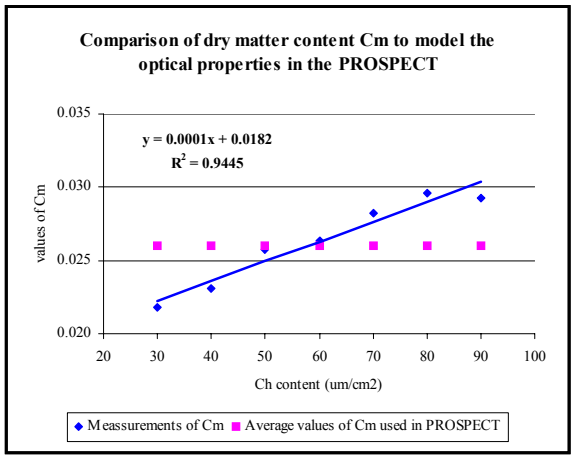

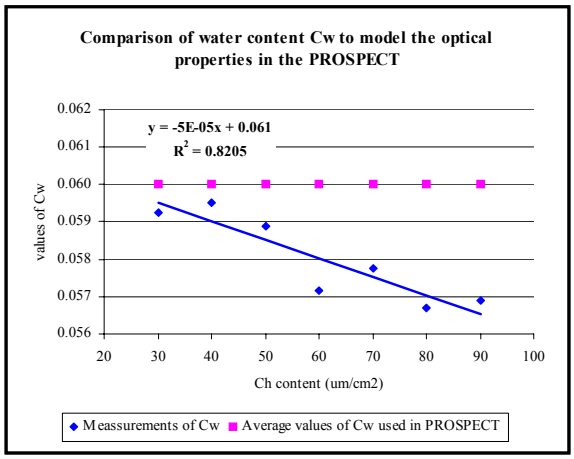

Appendix 10. Optical properties of representative elements used to create a realistic Norway spruce forest stand.

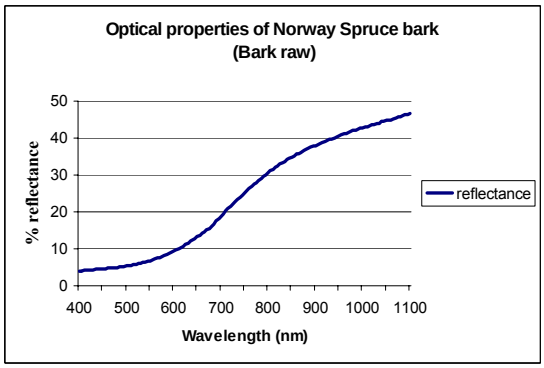

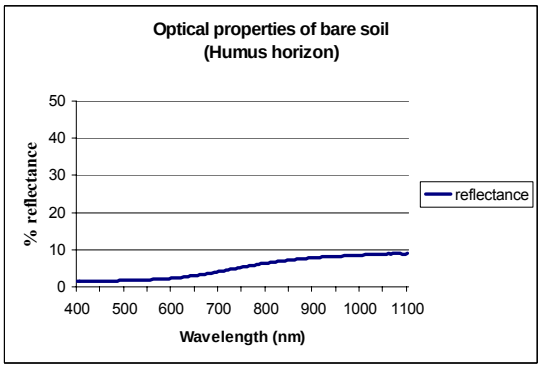

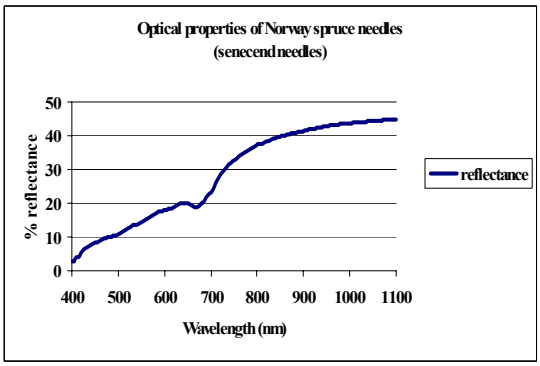

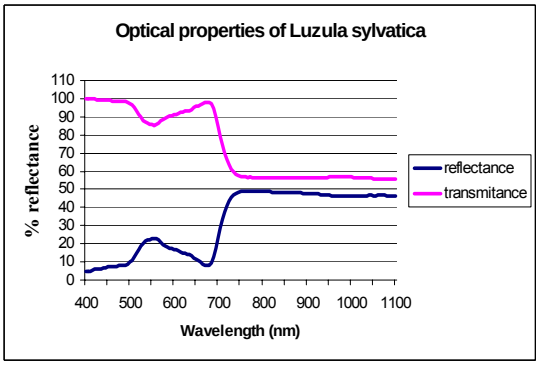

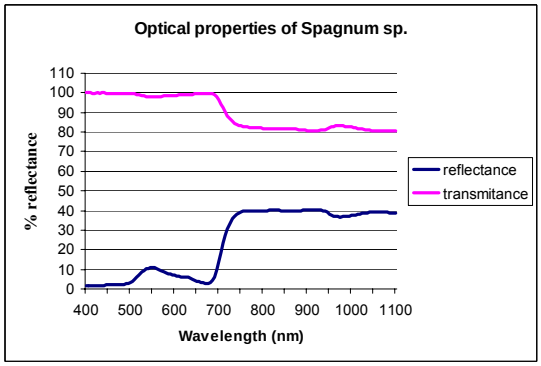

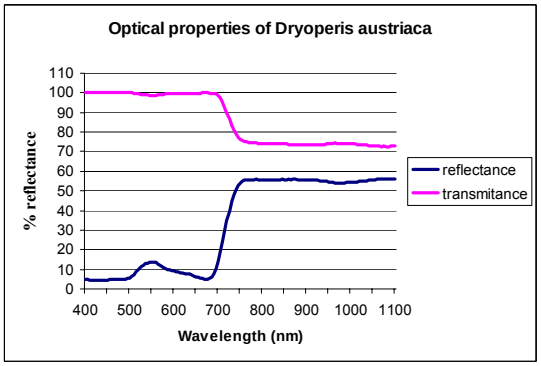

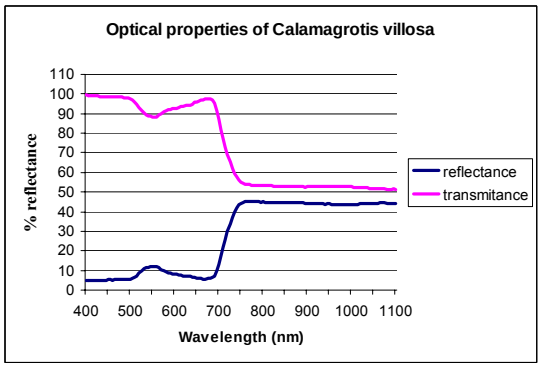

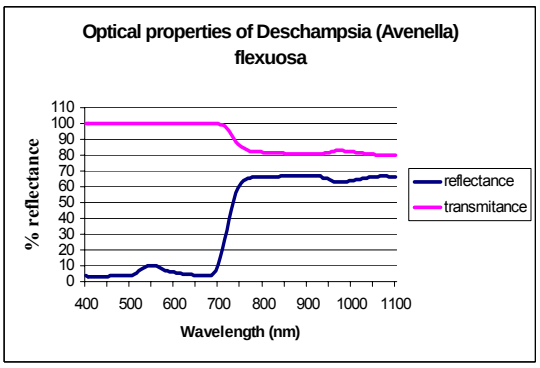

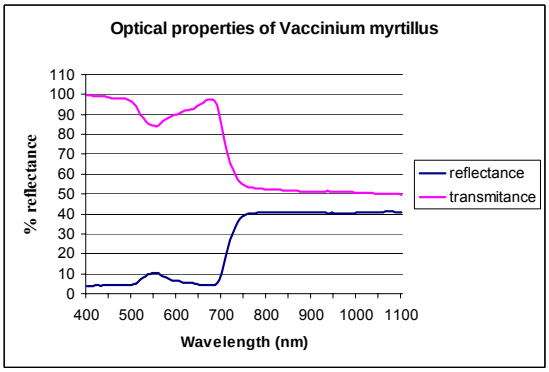
Optical properties of Vaccinium myrtillus
% reflectance
Wavelength (nm)
reflectance
transmitance

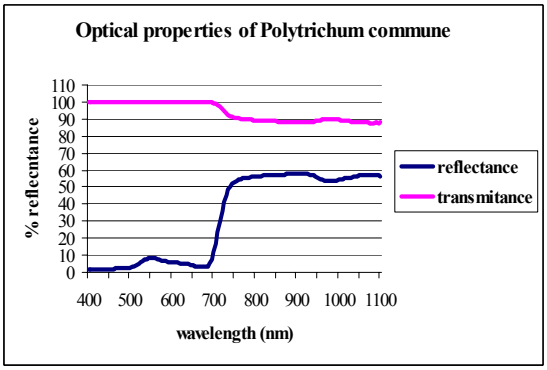
Optical properties of Polytrichum commune
% reflectance
wavelength (nm)
reflectance
transmitance

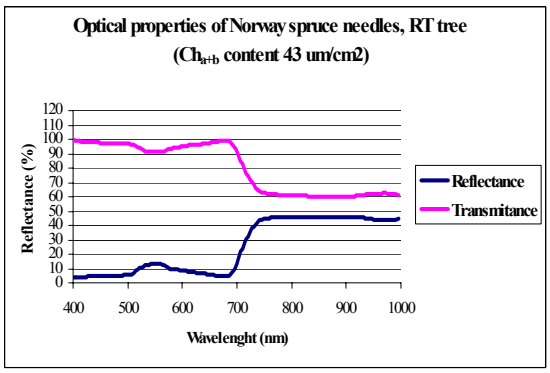
Optical properties of Norway spruce needles, RT tree
(Cha+b content 43 um/cm2)
Reflectance (%)
Wavelenght (nm)
Reflectance
Transmitance

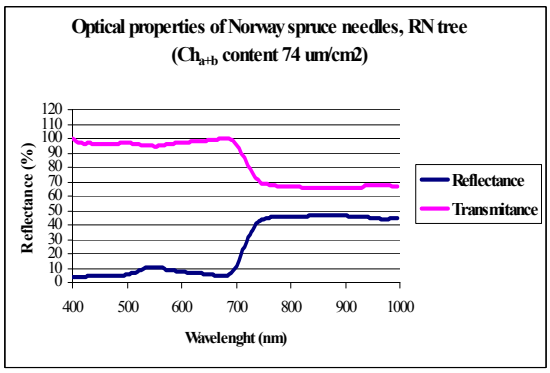
Optical properties of Norway spruce needles, RN tree
(Cha+b content 74 um/cm2)
Reflectance (%)
Wavelenght (nm)
Reflectance
Transmitance

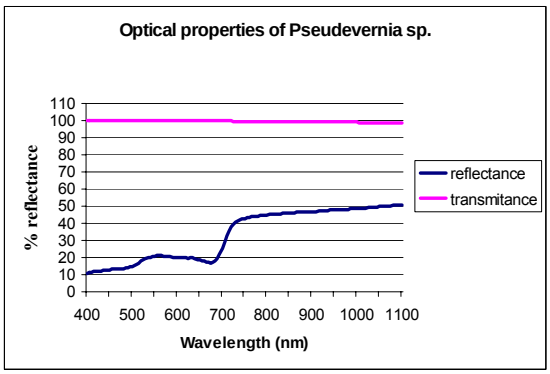
Optical properties of Pseudevernia sp.
% reflectance
Wavelength (nm)
reflectance
transmitance

Appendix 11. Hyperspectral images simulated by the DART model, the RGB colour composition of investigated forest stands (scenario 1).

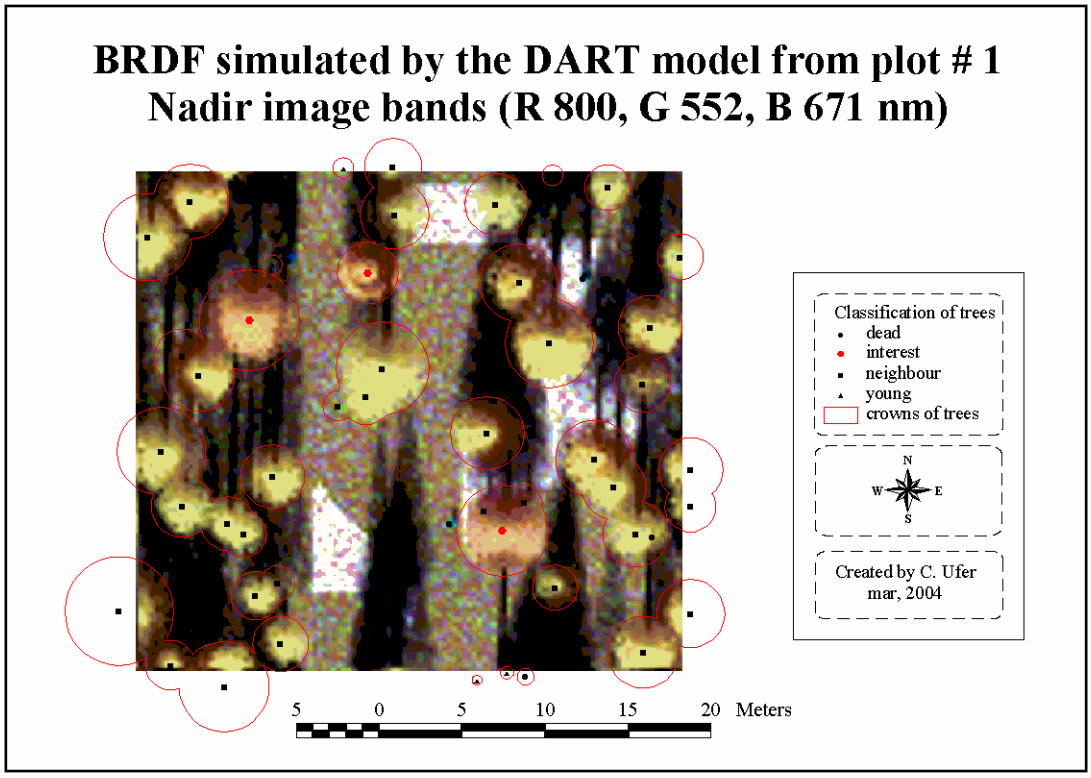

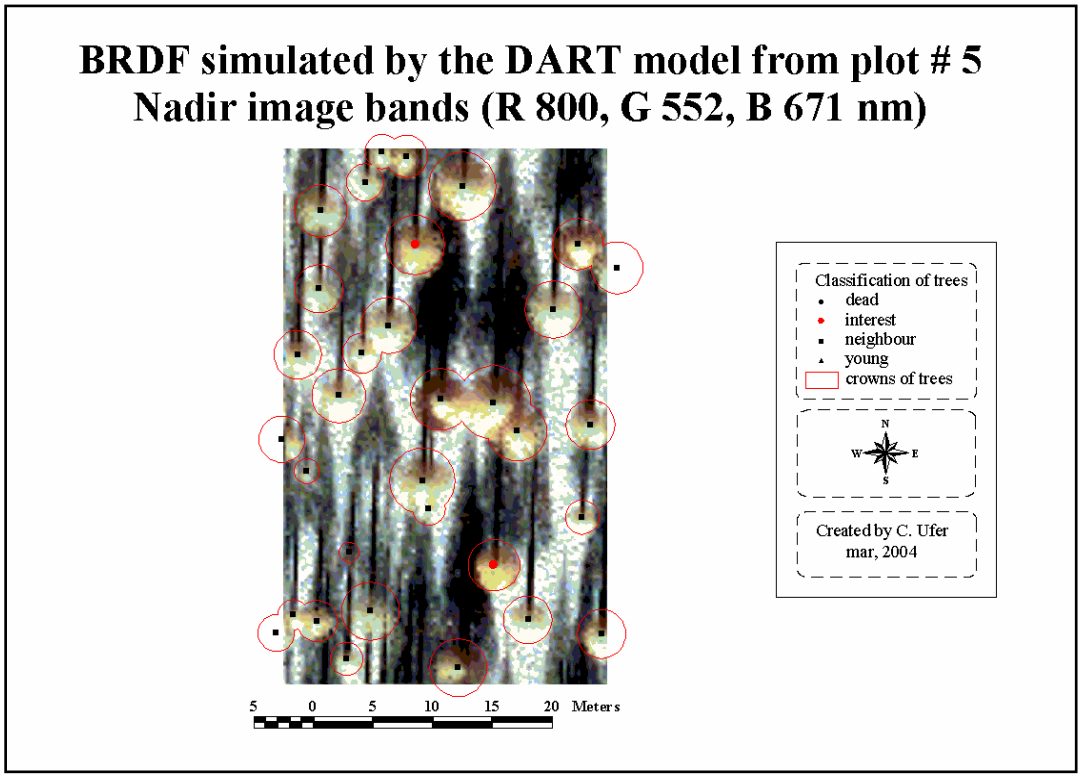

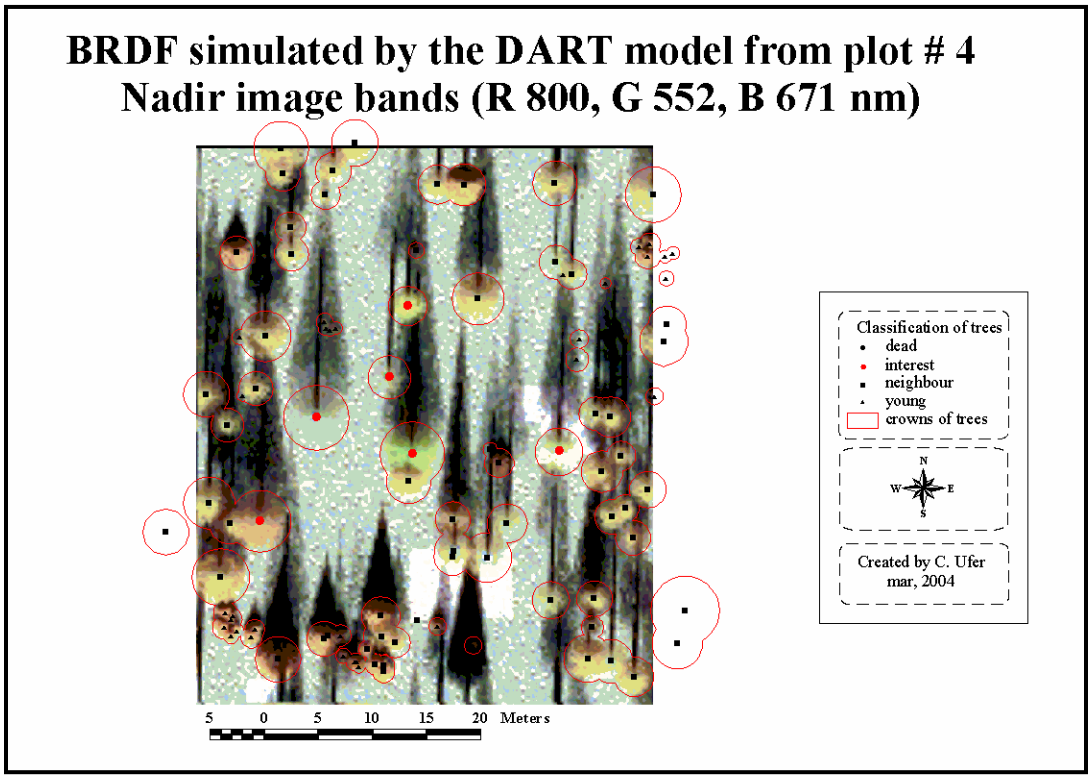

Appendix 12. Hyperspectral images simulated by the DART model, a RGB colour composition of the temporal research plot # 4 (scenario 2).

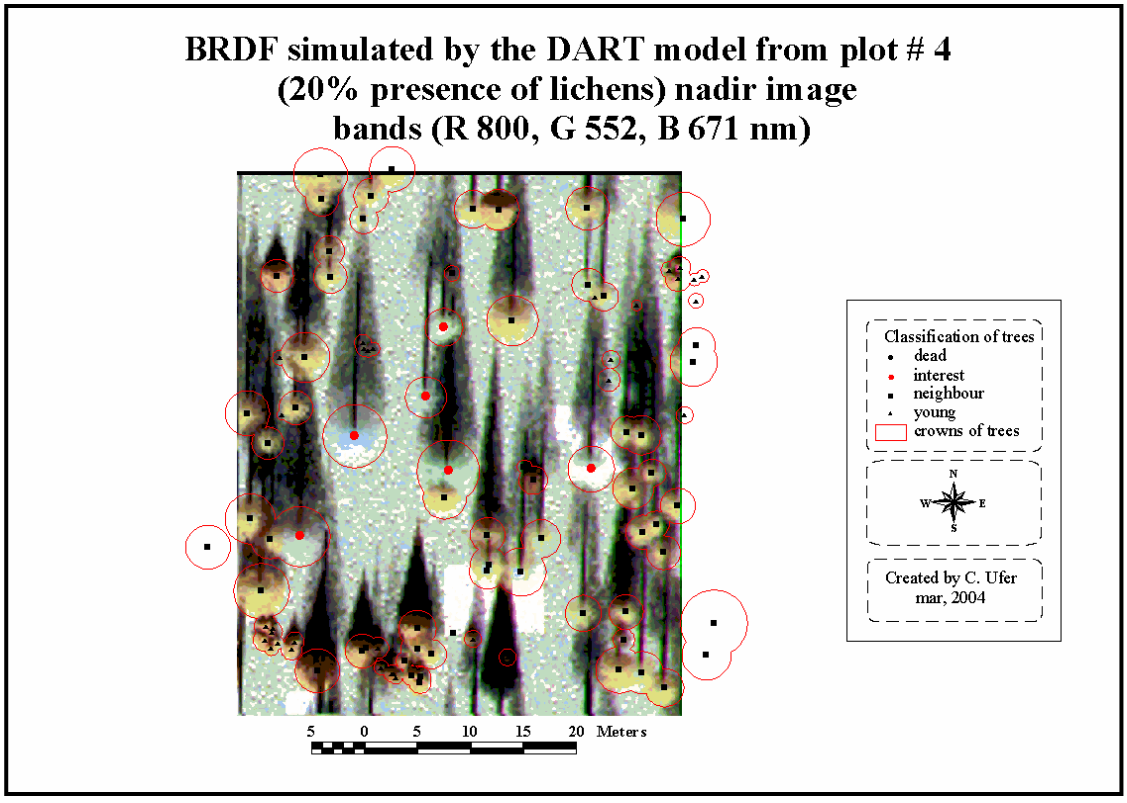

Appendix 13. Comparison between measured and retrieved Ch_{a+b} content using up-scaling methods (optical indices, merit functions and neural networks).

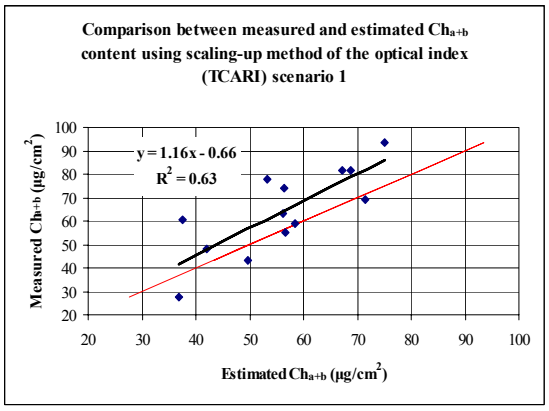

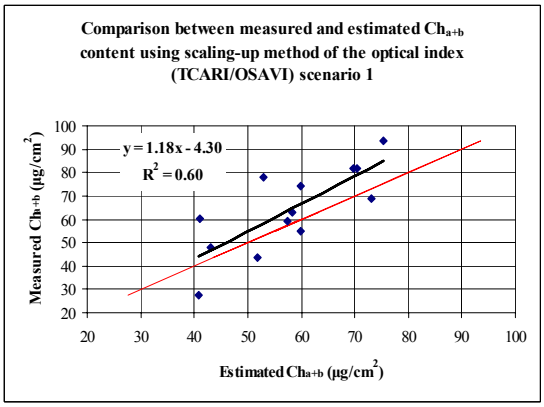

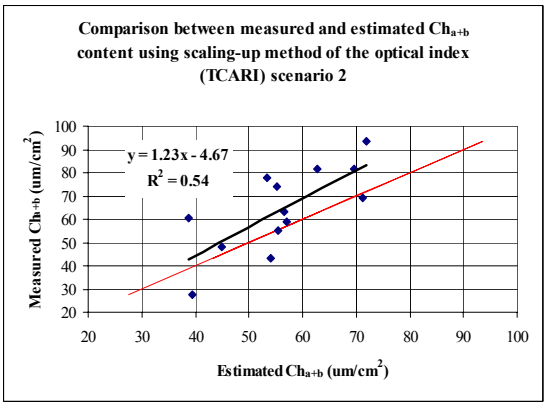

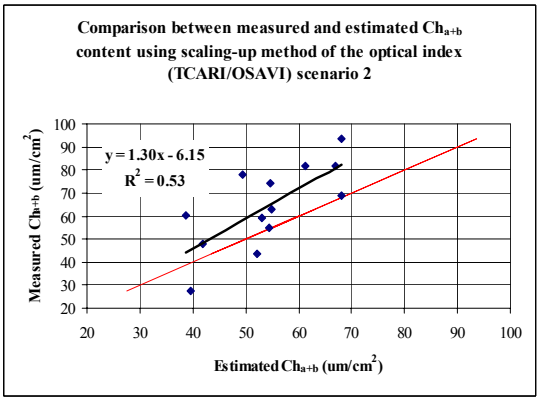

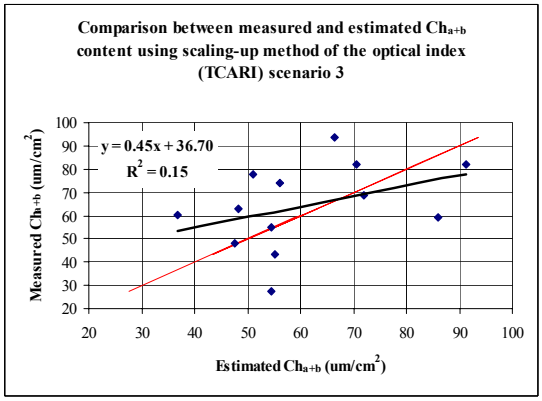

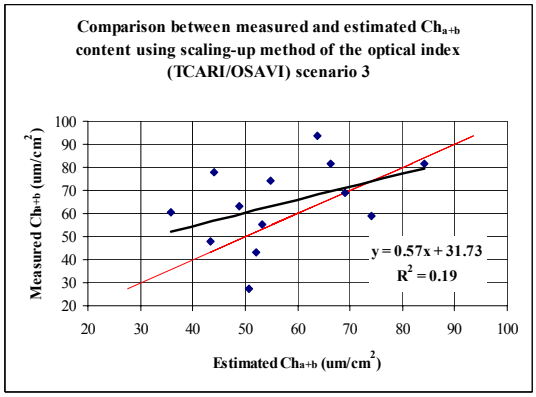

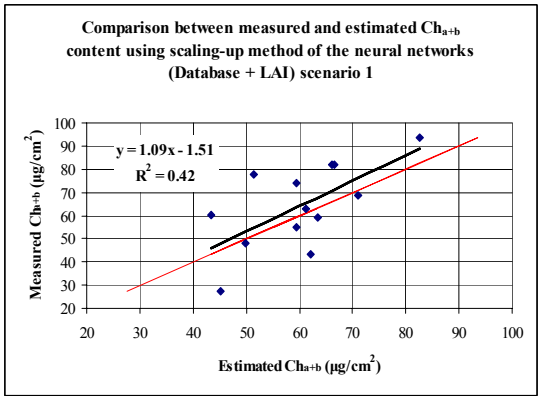
Comparison between measured and estimated Cha+b content using scaling-up method of the neural networks (Database + LAI) scenario 1
y = 1.09x - 1.51
R2 = 0.42
Measured Cha+b (µg/cm2)
Estimated Cha+b (µg/cm2)

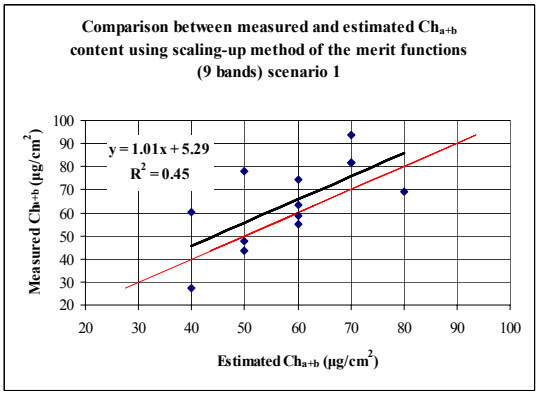
Comparison between measured and estimated Cha+b content using scaling-up method of the merit functions (9 bands) scenario 1
y = 1.01x + 5.29
R2 = 0.45
Measured Cha+b (µg/cm2)
Estimated Cha+b (µg/cm2)

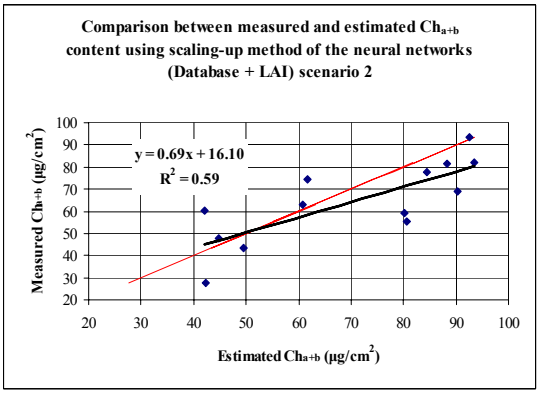
Comparison between measured and estimated Cha+b content using scaling-up method of the neural networks (Database + LAI) scenario 2
y = 0.69x + 16.10
R2 = 0.59
Measured Cha+b (µg/cm2)
Estimated Cha+b (µg/cm2)

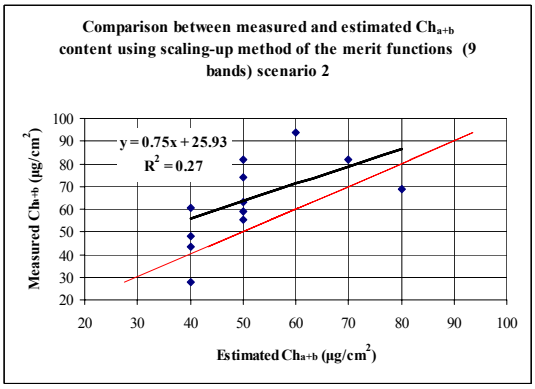
Comparison between measured and estimated Cha+b content using scaling-up method of the merit functions (9 bands) scenario 2
y = 0.75x + 25.93
R2 = 0.27
Measured Cha+b (µg/cm2)
Estimated Cha+b (µg/cm2)

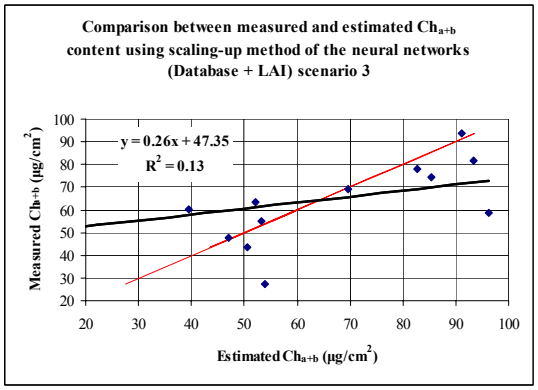
Comparison between measured and estimated Cha+b content using scaling-up method of the neural networks (Database + LAI) scenario 3
y = 0.26x + 47.35
R2 = 0.13
Measured Cha+b (µg/cm2)
Estimated Cha+b (µg/cm2)

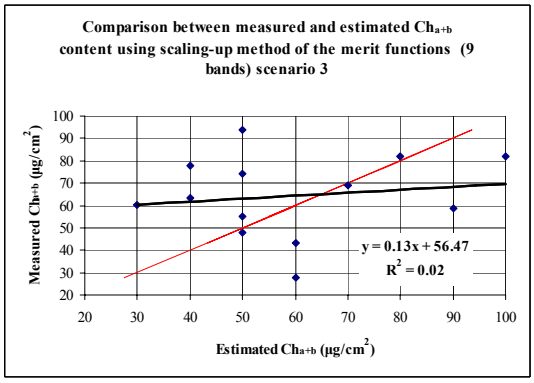
Comparison between measured and estimated Cha+b content using scaling-up method of the merit functions (9 bands) scenario 3
y = 0.13x + 56.47
R2 = 0.02
Measured Cha+b (µg/cm2)
Estimated Cha+b (µg/cm2)